Master's Thesis

Research on Reflective Semiconductor Optical Amplifier and Its Application in Wavelength Division Multiplexed Passive Optical Network

（反射型半導体光増幅器と波長多重パッシブ光ネットワークにおける応用に関する研究）

Zeng Yuxiao (37-116937)
Supervisor: Professor Yoshiaki Nakano

Department of Electrical Engineering and Information Systems,
School of Enginerring, The University of Tokyo

August 2013

Contents

Chapter 1

Introduction

1.1 Background

The demand for network bandwidth is increasing rapidly in recent years because of the explosive development in internet applications. Many studies have been done on different kinds of communication devices and network configurations, both in the *core network*, which is the central network that connects to other central networks in other areas or countries, and in the *access network*, which connects the service provider to business and residential subscribers.

Conventional solutions like digital subscriber line (DSL), cable modem (CM) and community antenna television (CATV) are still widely used in access networks, because the underlying infrastructures are already built and thus costs are relatively low. However, their network performance is poor and can hardly satisfy the needs of current end users.

Comparing with traditional copper-based network technology, optical networks can provide much higher bandwidth and have the advantage of immunity to electrical interference, and thus has been widely deployed in backbone networks. The deployment of optical access networks is slower, however, due to the higher cost that end users need to pay. An inexpensive and scalable optical communication technology is required for the further development in access networks.

1.2 Passive Optical Network

Passive optical network (PON) is considered to be an attractive solution to the problem above. PON is a point-to-multipoint (P2MP) network with tree topology, consisting of an optical line terminal (OLT) located at the central office (CO) of a service provider

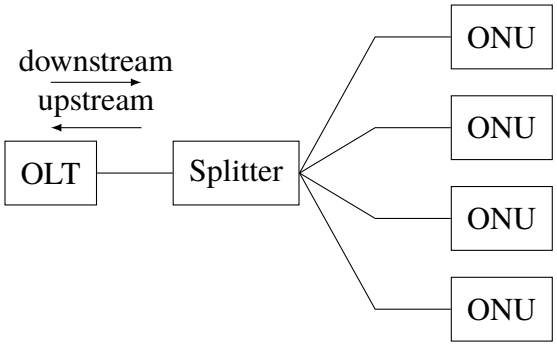

Figure 1.1: Network architecture of a TDM-PON such as GPON and EPON.

and optical network units (ONUs) in the field. A PON uses only unpowered passive optical components in the path from signals' source to destination, which eliminates the power use at CO and thus decreases the power consumption, making PON a cost-effective solution.

PON uses multiplexing technology to service multiple ONUs at the same time. There exist several standards for PONs utilizing time division multiplexing/time division multiple access (TDM/TDMA) technology. PONs utilizing wavelength division multiplexing (WDM) technology are being considered as a potential technology beyond current 10 Gbit/s TDMA PONs.

Before discussing details of different kinds of PONs, some terms need to be defined here. The transmission from OLT to ONU is in the *downstream* direction, and the transmission direction from ONU to OLT is referred to as *upstream*. A *feeder fiber* connects the OLT and the remote node (RN), and for each ONU there is a *distribution fiber* connecting it and the RN.

1.2.1 GPON and EPON

Gigabit passive optical network (GPON) is defined by IUT-T recommendation G.984. Ethernet passive optical network (EPON) is defined by IEEE 802.3ah. Both of GPON and EPON are TDM-PONs, and they have similar network architecture. As shown in Fig.1.1, a 1:N splitter is used to split the downstream signal from the OLT and to merge the upstream signals from the ONUs.

Upstream and downstream signals use different wavelength bands in a GPON or an EPON. In the downstream direction, network traffic is transmitted by the OLT and reach all ONUs. Then every ONU only takes the ones that are intended for him. However, a

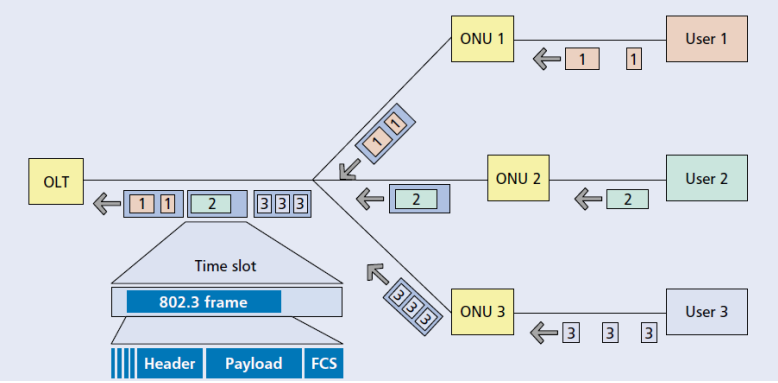

Figure 1.2: Upstream traffic in EPON [2].

malicious user can use his own ONU device to capture all downstream data. Encryption is used to protect the communication from being captured by other users. All these are done in the OLT under control of the central office.

Things becomes complicated for the upstream transmission. Upstream traffic is generated by all ONUs. Since all ONUs share one feeder fiber and one upstream wavelength, there must be some way to determine when one ONU should transmit the message so that the ONUs do not interfere each other. There is a common time reference generated by the OLT, and all ONUs are synchronized to that time reference. Transmission time slots are then determined from that time reference. Time slots can be allocated statically or dynamically, while they are usually allocated dynamically based on the bandwidth needs from ONUs, because the static scheme may cause great bandwidth waste. Several dynamic bandwidth allocation (DBA) algorithms exist to make maximum use of the network bandwidth [1].

The major difference between GPON and EPON is the frame format. EPON uses the Ethernet frame (802.3 frame) as the framing sublayer, as shown in Fig.1.2, while GPON uses its own framing protocol. Therefore an EPON is considered as a better choice to interconnect Ethernet networks than GPON [2].

There are some other differences between GPON and EPON, such as wavelength band choices, encryption methods and so on. GPON is being deployed in North America and Europe, while EPON is widely used in Asia. The 10 Gbit/s solutions of GPON and EPON are also defined recently, namely ITU-T G.987 XG-PON and IEEE 802.3av 10 GE-PON. [3]–[5]

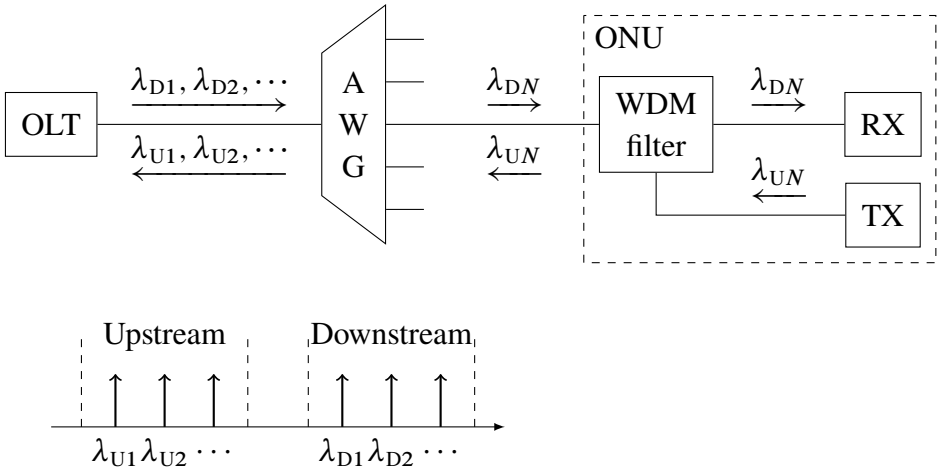

Figure 1.3: A simple architecture of a WDM-PON. RX: receiver; TX: transmitter; AWG: arrayed waveguide grating.

1.2.2 WDM-PON

In a WDM-PON, different wavelengths are used instead of different time slots to avoid the collision of communication between the OLT and different ONUs. A simple architecture of a WDM-PON is shown in Fig.1.3. Each ONU has his own downstream wavelength and upstream wavelength, denoted as λ_{DN} and λ_{UN} respectively for the N-th ONU. There is an arrayed waveguide grating (AWG) at the RN which is used to demultiplex the downstream signals and to multiplex the upstream signals. The wavelengths are chosen so that light at λ_{DN} and λ_{UN} can pass the N-th port of the AWG.

Although a WDM-PON is a P2MP network physically, the use of AWG and the allocation of different wavelength bands ensure that the connection between each ONU and the OLT is a point-to-point (P2P) one logically. As a result, a WDM-PON has several advantages over a TDM-PON, such as

- Security. It is difficult for an user to capture other users' data from any output port of the AWG.

- Ease of network management. Changes made to one user do not interrupt other users.

- Protocol and bit-rate transparency.

1.3 Options of Light Sources for ONU

While WDM-PON was proposed in the late 1980s [6], the research on it becomes popular in the recent 10 years because of the progress in AWGs and light sources. There are several choices in light sources, and the reviews for light sources used at ONUs are given as follows.

1.3.1 DFB-LD

Distributed feedback (DFB) laser diode (LD) is a favorable option for WDM communication. Distributed Bragg gratings are used instead of reflective mirrors in Fabry-Perot LDs to provide better wavelength filtering characteristics. DFB-LDs have narrow linewidth and good modulation property. They are mature and have been already widely used in lightwave systems.

However, DFB-LDs are considered as a costly option in WDM-PONs. Wavelength control is important in WDM communications. The wavelength of a DFB-LD is dependent on the temperature, and therefore a thermoelectric cooler (TEC) is required to stabilize the laser's operation. A wavelength locker is also needed to help the laser to lock to its assigned wavelength. That says, a DFB-LD itself is expensive.

The use of DFB-LDs in a WDM-PON also increases the cost in network management. Different ONUs need DFB-LDs operating at different wavelengths, that means, DFB-LD is a kind of *colored* light source. Backups of all ONUs are also needed in case some are in an unusable condition, while some others may never be used.

1.3.2 Injection-locked FP-LD

A Fabry-Perot (FP) laser diode is a multimode laser which generates light of many wavelength components. Frequency chirping exists when the FP-LD is directly modulated, and it will degrade the performance of the system greatly. However, when an external continuous-wave (CW) light is injected into the cavity, the FP-LD is forced to oscillate at the frequency of the external light, and the frequency chirping is reduced significantly. This property is called injection-locking. [7]

In order to use injection-locking FP-LDs in a WDM-PON, an external driving light source is needed. A spectrum-sliced broadband light source is used to provide the external light injection. The network architecture is shown in Fig.1.4. Field test on this kind of WDM-PON is done and showed good results [8].

Injection-locked FP-LD is considered as a economic light source of the ONU. It is

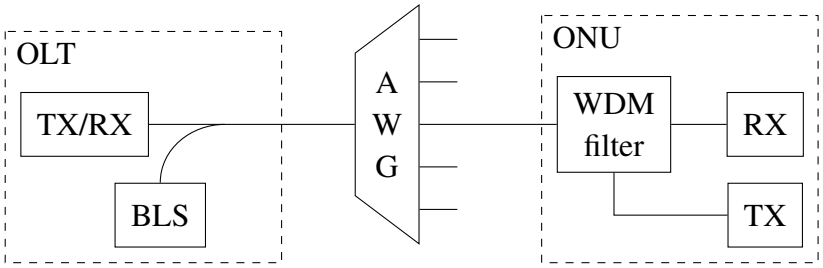

Figure 1.4: Architecture of a WDM-PON using a broadband light source (BLS) at the OLT to provide spectrum sliced ASE for the transmitter (TX) at the ONUs. The TX of the ONU can be an FP-LD or an RSOA.

colorless, meaning a common type of FP-LD can be used at all ONUs. However, the additional broadband light source required at the OLT introduces some extra cost. The use of injection locking method also requires some extra effort on control of modulation index, laser bias current, and power of external optical excitation [8].

1.3.3 Wavelength-seeding RSOA

Reflective semiconductor optical amplifier (RSOA) is another option for the light source at ONUs. The structure of an RSOA is similar to an FP-LD, with one exception that the two facets of FP-LD have high-reflection (HR) coatings, while one facet of RSOA has HR coating and the other has anti-reflection (AR) coating. Light enters the active medium of the RSOA from its AR facet, is amplified twice in the active medium (forwards and backwards), and then exits the RSOA from the AR facet.

RSOA can be used in the same network architecture as that of FP-LD. In Fig.1.4, the RSOA is used as the transmitter of the ONU [9]. It has two functions. The first function is to amplify the spectrum sliced light from the broadband light source at the OLT, which is called seeding light. Electric signal is applied directly to the RSOA, and therefore its second function is to modulate the seeding light.

RSOAs used in this way are called directly-modulated wavelength-seeding RSOA. It has a similar position in the network to that of an injection-locked FP-LD, while the working principles are different. Wavelength-seeding RSOA is also a kind of colorless transmitter.

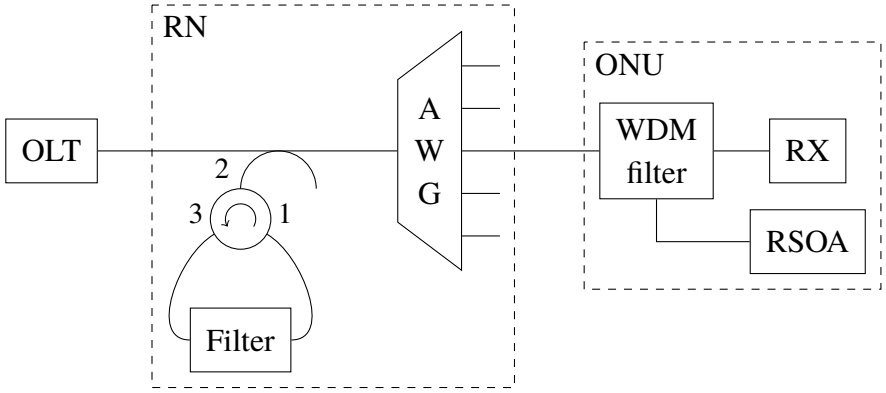

Figure 1.5: Architecture of a WDM-PON using self-seeding RSOA.

1.3.4 Self-seeding RSOA

Another way to use RSOAs in a WDM-PON is proposed by Wong, Lee, and Anderson in [10]. The network architecture is shown in Fig.1.5. Instead of using an additional broadband light source at the OLT, this kind of network creates a reflective path at the RN. The distribution fiber, the reflective path and the HR coating facet of the RSOA effectively form a cavity. The reflective path is composed of a circulator and a bandpass filter in the original paper, as shown in Fig.1.5, but it can also be consisted of a Faraday rotator mirror [11] or some other optical devices.

The reflective path leads to two important conclusions. The first one is the wavelength selection mechanism in the system. Consider the turn-on process of the RSOA. At first, no data is modulated on the RSOA and only amplified spontaneous emission (ASE) light from the RSOA exists in the fiber. ASE light, which has a wide bandwidth, is filtered by the WDM filter and the AWG. Consequently its spectrum will have a peak, the center wavelength of which is determined by the passive components in the optical path. The filtered light propagates back and is amplified by the RSOA. The amplified light is again filtered and amplified. The process repeats for several times, and finally the spectrum will become stable and a narrow peak is generated. The wavelength selection mechanism is called *self-seeded* because no external light is involved in this process.

The second conclusion is about the remodulation noise. We have seen that in the turn-on process, light emitted by the RSOA will propagate back to the RSOA and get amplified. The same applies to the modulated light. In real applications such FTTx (Fiber to the x, where x represents building, curb, home or premises), the distribution fiber can be 1 km long or more, and the round-trip time will be about 20 µs for example. The process of writing new data is in fact the process of remodulating data that was sent 20 µs

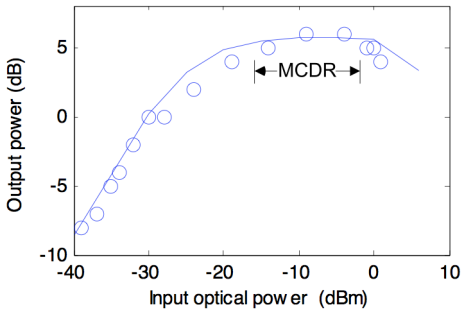

Figure 1.6: Input-output power transfer characteristic of an RSOA. When input power becomes large, the output power may decrease with the increase of input power. Open circle: experimental data; solid line: simulation result. [13]

ago. Therefore, in theory this kind of system suffers from the remodulation noise and can only afford low transmission rate of several tens of kilohertz.

Despite the poor performance predicted by theoretical analysis, experiments have shown different results. 1.25 Gbit/s [10], 2.5 Gbit/s and even 5 Gbit/s [12] operations have been demonstrated experimentally.

O'Duill, Marazzi, Palolari, *et al.* have pointed out in [13] that gain saturation phenomenon in RSOA makes the remodulation at high speed possible. Gain saturation is enhanced in RSOA comparing with usual single-pass SOA because of the cross-gain saturation phenomenon. Consequently, the output power of an RSOA will experience a reduction if the input power increases more as shown in Fig. 1.6. There exists a range for the input power that output power remains nearly constant if the input power varies in this range. If the reflected data signal falls in this range, the output will be almost continuous wave (CW), and thus the original modulation is cancelled. This range is called modulation-cancellation dynamic range (MCDR) therefore.

Clearly, self-seeding RSOA is also a kind of colorless transmitter. The cost of the WDM-PON using a self-seeding RSOA as the ONU transmitter is considered to be lower than those of the previous two kinds since the self-seeding operation eliminates the need of a power-consuming broadband light source. This kind of WDM-PON also has great temperature stability as shown in Fig.1.7 [14].

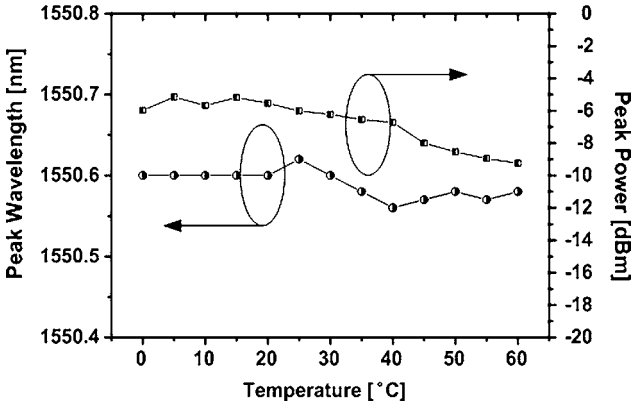

Figure 1.7: Temperature stability of self-seeding RSOA. [14]

1.4 Purpose of This Research

The WDM-PON solution using self-seeding RSOAs as colorless ONU transmitters is considered a cost-efficient solution in the near future. In spite of successful experiment demonstrations, the relationship between network performance and the characteristics of the RSOA still remains unknown. In order to release the full potential of this kind of WDM-PON, a detailed research on the only active device, the RSOA, is required. In addition, a theoretical direction on how to improve the network performance is also needed.

The purpose of this research is to give a solution to the problems mentioned above. We propose a numerical model for characterising RSOAs. Using this model, we can explain some experimental results and predict what kind of RSOA is suitable for the self-seeded WDM-PON application.

1.5 Outline of This Thesis

This thesis presents a numerical model for RSOA. Then a theory about the self-seeding method and supporting experimental results are presented.

The basic theory used to describe the dynamic process inside an RSOA is represented in Chapter 2. A numerical calculation method is introduced in Chapter 3. Experiments on RSOA and its application as a colorless directly-modulated self-seeding transmitter are shown in Chapter 4. A theory on the self-seeding method and some optimization proposals on the RSOA are represented in Chapter 5. Chapter 6 will summarize this thesis.

Chapter 2

Theory

In this chapter, I will introduce the basic theory, the rate equation that is used to analyze RSOAs. The rate equation consists of the wave propagating equation, the carrier density continuity equation and the gain equation.

2.1 Wave Equation

An RSOA has almost the same structure as that of a FP-LD, and therefore the analysis method is also similar. In order to describe the propagation of light inside an RSOA, we should use the Maxwell equations.

$$\nabla \times \mathbf{E} = -\frac{\partial \mathbf{B}}{\partial t} \tag{2.1}$$

$$\nabla \times \mathbf{H} = \mathbf{J} + \frac{\partial \mathbf{D}}{\partial t} \tag{2.2}$$

$$\nabla \cdot \mathbf{D} = \rho_{\mathrm{V}} \tag{2.3}$$

$$\nabla \cdot \mathbf{B} = 0 \tag{2.4}$$

in which $\mathbf{E}$ is the electric field vector, $\mathbf{H}$ is the magnetic field vector, $\mathbf{D}$ is the electric displacement field vector, $\mathbf{B}$ is the magnetic flux density vector, $\mathbf{J}$ is the current density vector and ρ_{V} is the charge density. For a nonmagnetic dielectric medium, these quantities have the following relationship,

$$\mathbf{D} = \varepsilon_0 \mathbf{E} + \mathbf{P} \tag{2.5}$$

$$\mathbf{B} = \mu_0 \mathbf{H} \tag{2.6}$$

$$\mathbf{J} = \sigma \mathbf{E} \tag{2.7}$$

in which ε_0 and μ_0 are the vacuum permittivity and vacuum permeability respectively, $\mathbf{P}$ is the electric polarization vector, and σ is the conductivity of the medium.

However, the Maxwell equations are too difficult to solve, and therefore we need some approximations to simplify them. Assuming the media is simple (homogeneous and isotropic) and there is no free charge ($\rho_{\mathrm{V}} = 0$), we can obtain

$$\begin{aligned}\nabla \times \nabla \times \mathbf{E} &= -\mu_0 \frac{\partial}{\partial t}(\nabla \times \mathbf{H}) \\ &= -\mu_0 \frac{\partial \mathbf{J}}{\partial t} - \mu_0 \frac{\partial^2 \mathbf{D}}{\partial t^2} \\ &= -\mu_0 \sigma \frac{\partial \mathbf{E}}{\partial t} - \mu_0 \varepsilon_0 \frac{\partial^2 \mathbf{E}}{\partial t^2} - \mu_0 \frac{\partial^2 \mathbf{P}}{\partial t^2}\end{aligned} \tag{2.8}$$

At the same time, using the approximation

$$\nabla \cdot \mathbf{E} = 0 \tag{2.9}$$

we have

$$\begin{aligned}\nabla \times \nabla \times \mathbf{E} &= \nabla(\nabla \cdot \mathbf{E}) - \nabla^2 \mathbf{E} \\ &= -\nabla^2 \mathbf{E}\end{aligned} \tag{2.10}$$

Therefore

$$\nabla^2 \mathbf{E} - \mu_0 \sigma \frac{\partial \mathbf{E}}{\partial t} - \mu_0 \varepsilon_0 \frac{\partial^2 \mathbf{E}}{\partial t^2} = \nabla^2 \mathbf{E} - \frac{\sigma}{\varepsilon_0 c^2} \frac{\partial \mathbf{E}}{\partial t} - \frac{1}{c^2} \frac{\partial^2 \mathbf{E}}{\partial t^2} = \frac{1}{\varepsilon_0 c^2} \frac{\partial^2 \mathbf{P}}{\partial t^2} \tag{2.11}$$

Here we have used the relation

$$\mu_0 \varepsilon_0 = \frac{1}{c^2} \tag{2.12}$$

where c is the speed of light in vacuum.

For time-harmonic electromagnetic fields, the complex notation is more useful and more convenient than the time-domain representation. Assuming the electromagnetic field is time-harmonic, we have

$$\mathbf{E}(x, y, z, t) = \mathrm{Re}\{\tilde{\mathbf{E}}(x, y, z) \exp(-i\omega t)\} \tag{2.13}$$

$$\mathbf{P}(x, y, z, t) = \mathrm{Re}\{\tilde{\mathbf{P}}(x, y, z) \exp(-i\omega t)\} \tag{2.14}$$

where ω is the angular frequency of the electromagnetic field.

Using the complex notation, equation (2.11) can be rewritten as

$$\nabla^2 \tilde{\mathbf{E}} + k_0^2 \left(1 + \frac{i\sigma}{\varepsilon_0 \omega}\right) \tilde{\mathbf{E}} = -\frac{k_0^2}{\varepsilon_0} \tilde{\mathbf{P}} \tag{2.15}$$

where $k_0 = \omega/c$ is the wavenumber in vacuum.

Usually the intraband scattering processes in semiconductor is relatively fast than other interesting time scales like the photon lifetime and the carrier recombination time. Therefore we can assume that the response of polarization $\mathbf{P}$ to external electric field $\mathbf{E}$ is instantaneous, that is,

$$\tilde{\mathbf{P}} = \varepsilon_0 \chi(\omega) \tilde{\mathbf{E}} \tag{2.16}$$

where χ is the susceptibility of the material and it is frequency-dependent. χ can be decomposed into two parts

$$\chi = \chi_0 + \chi_p \tag{2.17}$$

where χ_0 is the medium susceptibility in the absence of external pumping and χ_p is the additional contribution to the susceptibility related to the strength of pumping. For RSOAs, the source of pumping the current injection, and χ_p depends on the concentration of charge carriers in the active layer.

Using (2.16), (2.15) becomes

$$\nabla^2 \tilde{\mathbf{E}} + k_0^2 \left(1 + \frac{i\sigma}{\varepsilon_0 \omega}\right) \tilde{\mathbf{E}} + k_0^2 \chi \tilde{\mathbf{E}} = \nabla^2 \tilde{\mathbf{E}} + \varepsilon k_0^2 \tilde{\mathbf{E}} = 0 \tag{2.18}$$

where the complex dielectric constant ε is defined as

$$\begin{aligned} \varepsilon &= 1 + \chi + \frac{i\sigma}{\varepsilon_0 \omega} \\ &= 1 + \chi_0 + \chi_p + \frac{i\sigma}{\varepsilon_0 \omega} \\ &= n_b^2 + \varepsilon' \end{aligned} \tag{2.19}$$

in which $n_b = \sqrt{1 + \mathrm{Re}\{\chi_0\}}$ is the background refractive index of the unpumped material, and ε' is the rest part of ε.

Finally, we transform (2.18) to its time-domain representation and get

$$\nabla^2 \mathbf{E} - \frac{\varepsilon}{c^2} \frac{\partial^2 \mathbf{E}}{\partial t^2} = 0 \tag{2.20}$$

This equation is called wave equation. [7]

2.2 Rate Equation I - Wave Propagation

The wave equations is still to complexed to solve, and we need some further approximations. A common approximation is the slowly-varying envelope approximation (SVEA).

Under SVEA, the electric field is assumed to be linearly polarized the also remains linearly polarized during propagation. Therefore the electric field propagating forwards can be written as

$$\mathbf{E}(x, y, z, t) = \mathbf{F}(x, y)A(z, t)e^{i(kz-\omega t)} \tag{2.21}$$

where $\mathbf{F}(x, y)$ is the waveguide-mode distribution, $A(z, t)$ is the envelope, $k = k_0 n_{\text{eff}}$ is the wavenumber in the material, and n_{eff} is the effective refractive index.

Substituting (2.21) in (2.20), we obtain

$$\left(\frac{\partial^2}{\partial x^2} + \frac{\partial^2}{\partial y^2}\right)\mathbf{F} \cdot Ae^{i(kz-\omega t)} + \mathbf{F} \cdot \left(-k^2 A + ik\frac{\partial}{\partial z}A + \frac{\partial^2}{\partial z^2}A\right) \cdot e^{i(kz-\omega t)} = \frac{\varepsilon}{c^2}\mathbf{F} \cdot \left(-\omega^2 A - i\omega\frac{\partial}{\partial t}A + \frac{\partial^2}{\partial t^2}A\right)e^{i(kz-\omega t)} \tag{2.22}$$

The waveguide-mode distribution should satisfy the following equation.

$$\frac{\partial^2 \mathbf{F}}{\partial x^2} + \frac{\partial^2 \mathbf{F}}{\partial y^2} + (n_b^2 - n_{\text{eff}}^2)\frac{\omega^2}{c^2}\mathbf{F} = \mathbf{0} \tag{2.23}$$

Under SVEA, the change in envelope $A(z, t)$ is not fast, and therefore we can neglect the second derivatives of $A(z, t)$ in (2.22). Using (2.23), we have

$$k\frac{\partial}{\partial z}A \cdot \mathbf{F} + \frac{\varepsilon\omega}{c^2}\frac{\partial}{\partial t}A \cdot \mathbf{F} = ik_0^2\varepsilon' A \cdot \mathbf{F} \tag{2.24}$$

Multiplying $\mathbf{F}^*$ to both sides of (2.24) and integrating over x-axis and y-axis, we obtain

$$\frac{1}{v_g}\frac{\partial A}{\partial t} + \frac{\partial A}{\partial z} = GA \tag{2.25}$$

where v_g is the group velocity and G is the constant of integration.[15]

(2.25) describes the propagation of wave envelope. In a semiconductor active medium, it is convenient to decompose G into two parts

$$G = g - \alpha \tag{2.26}$$

where g is the gain from the medium, α is the material loss and G is the net gain. Thus for the electric field propagating forwards, we have

$$\frac{1}{v_g}\frac{\partial A^+}{\partial t} + \frac{\partial A^+}{\partial z} = (g - \alpha)A^+ \tag{2.27}$$

Gain g will be discussed later in this chapter.

Similarly, for the electric field propagating backwards, we can get

$$\frac{1}{v_g}\frac{\partial A^-}{\partial t} - \frac{\partial A^-}{\partial z} = (g - \alpha)A^- \tag{2.28}$$

2.3 Rate Equation II - Carrier Density

The carrier in semiconductor is electron and hole. Therefore in general we need two equations to describe the carrier densities, one for electron and one for hole. However, densities of electrons and holes are not independent because of charge neutrality. We will only consider the carrier density of electrons for simplicity.

We use $n(x, y, z, t)$ to represent the carrier density inside the cavity of RSOA. The value of n is generally dependent on the coordinates x, y and z, and it also changes with time t. The change in carrier density over time can be written as

$$\frac{\partial n}{\partial t} = \text{Diffusion} + \text{Injection} - \text{Recombination} \tag{2.29}$$

Next I will analyze the terms in the right hand.

2.3.1 Diffusion

The carrier diffusion is usually described by the following equation

$$\text{Diffusion} = D\nabla^2 n \tag{2.30}$$

where D is the diffusion coefficient. Comparing with the diffusion length, practical RSOA devices usually have much smaller active medium width and thickness, and therefore we can use treat n as an average value along the transverse dimensions.

Diffusion is still complicated after the approximation above. Based on the fact that the carrier density does not vary significantly over the length dimension of the active medium, the diffusion term can be assumed to be approximately constant and therefore it can be neglected from (2.29).

2.3.2 Injection

We use current injection on an RSOA device. The injection term can be written as

$$\text{Injection} = \frac{J}{qd} \tag{2.31}$$

where $q = 1.602 \times 10^{-19}$ C is the electron charge, and J is the current density which is defined as

$$J = \frac{I}{wL} \tag{2.32}$$

in which L is the length of the active region and I is the injection current.

2.3.3 Recombination

The recombination rate of RSOA can be generally decomposed into two parts, the recombination related to stimulated emission, and other recombination mechanisms.

RSOA amplifies light using the principle of stimulated emission. In (2.27) we have used g to represent the real gain from the active medium. The stimulated emission recombination rate R_{stim}, which is at the same time the photon generation rate, can be written as

$$R_{\text{stim}} = v_g g n_{\text{ph}} \tag{2.33}$$

where n_{ph} is the photon density. If the electric field envelope A is normalized such that $|A|^2$ represents the power of light, n_{ph} should have the following relationship with A,

$$|A|^2 = n_{\text{ph}} \cdot \hbar\omega \cdot w d v_g \tag{2.34}$$

in which $\hbar$ is the reduced Planck constant and $\hbar = 1.0546\,\text{J s}$.

Other recombination mechanisms include bimolecular recombination, Auger recombination and nonradiative recombination. They are related to the carrier density. Recombination rate caused by other recombination mechanisms can be written as

$$R(n) = A_{\text{nr}} n + B n^2 + C n^3 \tag{2.35}$$

where A_{nr} is the nonradiative recombination rate, B is the bimolecular recombination coefficient and C is the Auger recombination coefficient.

2.3.4 Complete Carrier Density Rate Equation

Using (2.29), (2.33) and (2.35), ignoring the diffusion term, we can write the complete carrier density rate equation. Including both the forward wave and the backward wave, it becomes

$$\frac{\partial n}{\partial t} = \frac{J}{qd} - v_g g (n_{\text{ph}}^+ + n_{\text{ph}}^-) - R(n) \tag{2.36}$$

2.4 Rate Equation III - Gain

Gain g was introduced in (2.27) as a part of constant of integration. The integration involves the calculation of susceptibility χ or the polarization vector $\mathbf{P}$. An exact calculation can be performed using quantum electronics theory, and it has been proved useful for gas and solid-state lasers. However, this method is not so useful for semiconductor lasers or RSOAs because of the complexity of the semiconductor material.

Generally a phenomenological approach is used in the analysis of semiconductor lasers and optical amplifiers. In this approach, the gain is assumed to have the following relationship with carrier density,

$$g = \Gamma a(n - n_0) \tag{2.37}$$

in which Γ is the optical confinement factor, a is the gain constant and n_0 is the transparency carrier density, meaning g will be 0 if $n = n_0$.

This assumption is successful to describe the characteristics of usual semiconductor lasers and single-pass optical amplifiers. However, it is not enough for RSOAs. Experiments show that RSOAs experience a strong gain saturation when input power is high, which is difficult to be explained using the existing theory. [13]

(2.37) needs to be modified to describe the operation of RSOA. We can notice that the main difference between a single-pass SOA and an RSOA is the optical waves inside the cavities. In a single-pass SOA, only forward wave exists in the cavity, while in an RSOA, both forward and backward traveling waves exist. A mutual effect may occur on the two traveling waves.

Based on this idea, we can modify equation (2.37) to include the mutual effect. The new gain equations consist of two equations and they are

$$g^+ = \frac{\Gamma a(n - n_0)}{1 + \varepsilon_{11} n_{\text{ph}}^+ + \varepsilon_{12} n_{\text{ph}}^-} \tag{2.38}$$

$$g^- = \frac{\Gamma a(n - n_0)}{1 + \varepsilon_{22} n_{\text{ph}}^- + \varepsilon_{21} n_{\text{ph}}^+} \tag{2.39}$$

in which g^+ and g^- are the gain experienced by the electric field propagating forwards E^+ and the electric field propagating backwards E^- respectively, ε_{11} and ε_{22} are self-gain saturation factors, and ε_{12} and ε_{21} are cross-gain saturation factors. It is usually assumed that $\varepsilon_{11} = \varepsilon_{22}$ and $\varepsilon_{12} = \varepsilon_{21}$. Since the cross-gain saturation is stronger than self-gain saturation, it is also assumed that $\varepsilon_{12} = 2\varepsilon_{11}$. [16]

2.5 Summary

The complete rate equation using the modified gain equation is given as following.

$$\frac{1}{v_g}\frac{\partial A^\pm}{\partial t} \pm \frac{\partial A^\pm}{\partial z} = (g^\pm - \alpha)A^\pm \tag{2.40}$$

$$\frac{\partial n}{\partial t} = \frac{J}{qd} - v_g(g^+ n_{\text{ph}}^+ + g^- n_{\text{ph}}^-) - R(n) \tag{2.41}$$

$$g^{\pm} = \frac{\Gamma a(n - n_0)}{1 + \varepsilon_{11} n_{\mathrm{ph}}^{\pm} + \varepsilon_{12} n_{\mathrm{ph}}^{\mp}} \tag{2.42}$$

in which

$$R(n) = A_{\mathrm{nr}} n + Bn^2 + Cn^3 \tag{2.43}$$

$$|A^{\pm}|^2 = n_{\mathrm{ph}}^{\pm} \cdot \hbar\omega \cdot w dv_g \tag{2.44}$$

Chapter 3

Numerical Simulation

In the previous I have derived the rate equation to describe the characteristics of an RSOA device. Although it is simpler than the original Maxwell equations and constitutive equations, it is still too complicated to solve by hand because it contains nonlinear terms. It becomes even harder under modulation condition.

In this chapter I will introduce a numerical simulation method to calculate the solution of the rate equation. I will first give a description of this method and a sample program structure, and then give the parameters needed upon numerical calculation.

3.1 Calculation Method

The rate equation is effectively a set of partial differential equations. There are many methods developed to solve partial differential equations numerically, like finite difference method, finite volume method and finite element method. [17]

In this research, I use a modified version of finite difference method to solve the rate equation. The first reason to use this method is its simplicity. It is based on the finite difference method, which is generally considered to be easier to implement than other methods. The second reason is that it can reveal the physical nature of the rate equation as we will see in the following derivation.

3.1.1 Discretization

The first step of this method is to discretizate the solution domain. The envelopes $A^{\pm}$ and the carrier density n are functions of the space coordinate z and time coordinate t. Instead of using continuous variables, we only consider $A^{\pm}$ and n on a discrete grid, as shown in Fig.3.1. The grid on z-axis has a definite point number because we are only

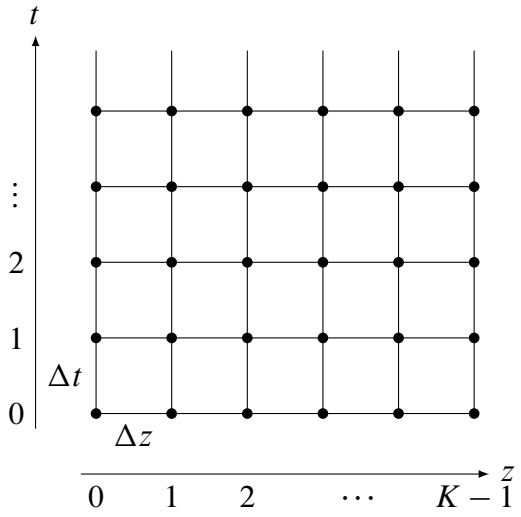

Figure 3.1: Grid for the discretization.

interested in the cavity of the RSOA which has a limited length, while the grid on t-axis has infinite points. If we use Δz and Δt to represent the mesh sizes of the grids on z-axis and t-axis respectively, we can write the discrete coordinates as

$$t[m] = m\Delta t, m = 0, 1, 2, \cdots \tag{3.1}$$

$$z[k] = k\Delta z, k = 0, 1, 2, \cdots, K-1 \tag{3.2}$$

where K is the number of grid points on z-axis and $K = L/\Delta z$. We choose Δt such that

$$\Delta t = \frac{\Delta z}{v_g} \tag{3.3}$$

Other variables are also discretizated. Afterwards we use the subscript and the number in brackets to represent the discrete space index and discrete time index respectively. For example,

$$A_k^+[m] = A^+(k\Delta z, m\Delta t) \tag{3.4}$$

3.1.2 Initial Condition

In real devices, there is spontaneous emission in the cavity. Therefore at first the electric field is not zero, and there is fluctuation in carrier density. However, these initial conditions have little effect after the RSOA device is injected with light and current that are much

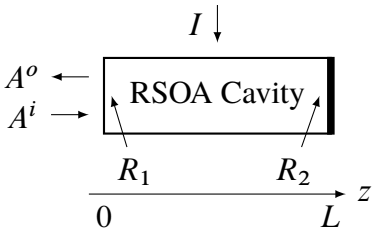

Figure 3.2: Some parameters and variables used in the numerical simulation.

stronger than initial distribution. Hence we use the simple initial condition as follows.

$$A_k^{\pm}[0] = -100 \text{ dBm} \tag{3.5}$$

$$n_k[0] = n_0 \tag{3.6}$$

3.1.3 Boundary Condition

Boundary condition is important in the analysis of RSOA, because it defines the difference between an RSOA and a laser, or an RSOA and a single-pass SOA. An RSOA device has an AR-coated facet and an HR-coated facet. In this research, we put the z-axis in such a way that the AR-coated facet is located at $z = 0$ and the HR-coated facet is located at $z = L$, as shown in 3.2,

On the HR-coated facet, we have the following boundary condition

$$A_{K-1}^{-}[m+1] = \sqrt{R_2} g_{K-1}^{+}[m] A_{K-1}^{+}[m] \tag{3.7}$$

in which R_2 is the reflectivity of the HR-coated facet. Here we use the square root of the reflectivity because reflectivity represents the ratio of power, while the envelope is a quantity like the electric field.

The reflectivity of the AR-coated facet should be 0 ideally. However, it is practically impossible to fabricate such a perfect facet. Here we consider the effect of the reflection on the imperfect AR-coated facet, and thus have the following boundary condition on the it

$$A_0^{+}[m+1] = \sqrt{R_1} g_0^{-}[m] A_0^{-}[m] + \sqrt{1-R_1} A^i[m+1] \tag{3.8}$$

where R_1 is the reflectivity of the AR-coated facet, and A^i is the envelope of the input light and should have the following relationship with the power of input light P_i

$$A^i[m] = \sqrt{P_i[m]} \tag{3.9}$$

3.1.4 Input and Output Variables

Here we refer to the quantities that may vary with time as *variables*, and other quantities as *parameters*. Input variables include the input light P_i or A^i, and the injection current J or I. We assume that the current is injected uniformly to the active region of the RSOA device.

Output variables include the internal electric field envelopes $A^{\pm}$ and the carrier density n. The envelope of the output light A^o is also an output variable, and it can be derived from the internal electric field using the following relationship

$$A^o[m+1] = \sqrt{1-R_1}\, g_0^-[m] A_0^-[m] \tag{3.10}$$

And the power of output light should be

$$P_o[m] = |A^o[m]|^2 \tag{3.11}$$

3.1.5 Finite Difference Method

Following finite difference method, we use discrete variables on grids instead of continuous variables. Accordingly, the differential of continuous variables are substituted by the difference quotients of discrete variables. There are several forms of difference quotients, that is, the forward, backward and central difference quotients. For example, the three kinds of difference quotients for $\partial A^+/\partial z$ are

$$(D_{\mathrm{f},z} A^+)(z) = \frac{A^+(z+\Delta z, t) - A^+(z,t)}{\Delta z} \tag{3.12}$$

$$(D_{\mathrm{b},z} A^+)(z) = \frac{A^+(z,t) - A^+(z-\Delta z, t)}{\Delta z} \tag{3.13}$$

$$(D_{\mathrm{c},z} A^+)(z) = \frac{A^+(z+\Delta z, t) - A^+(z-\Delta z, t)}{2\Delta z} \tag{3.14}$$

in which $D_{\mathrm{f},z}$, $D_{\mathrm{b},z}$ and $D_{\mathrm{c},z}$ are the forward, backward, central difference operator on z respectively.

Substituting differentials with any kind of difference quotients, we have the difference quotient version of rate equation. We further use discrete variables on grids instead of continuous variables and get completely discretizated rate equation. For instance, using

the forward difference, the rate equation becomes

$$\frac{1}{v_g}\frac{A_k^+[m+1]-A_k^+[m]}{\Delta t}+\frac{A_{k+1}^+[m]-A_k^+[m]}{\Delta z}=(g_k^+[m]-\alpha)A_k^+[m] \tag{3.15}$$

$$\frac{1}{v_g}\frac{A_k^-[m+1]-A_k^-[m]}{\Delta t}-\frac{A_{k+1}^-[m]-A_k^-[m]}{\Delta z}=(g_k^-[m]-\alpha)A_k^-[m] \tag{3.16}$$

$$\frac{n_k[m+1]-n_k[m]}{\Delta t}=\frac{J[m]}{qd}-v_g(g_k^+[m]n_{\mathrm{ph},k}^+[m]+g_k^-[m]n_{\mathrm{ph},k}^-[m])-R(n_k[m]) \tag{3.17}$$

I have tried to write a calculation program using the equations above. However, the program failed to give any useful results because the results do not converge. Adding grid number may help, but the calculation will become too slow. This kind of equations are called stiff partial differential equations. For the equations in this research, a plain finite difference method seems insufficient.

3.1.6 Modified Finite Difference Method

A detailed analysis on the previous calculation progress shows that the problem comes from the fast increase in $A^{\pm}$. Since $A^{\pm}$ are calculated in equations (3.15) and (3.16), the two equations may need a modification so that the results are convergent.

Now we go back to the wave propagation equation derived in Chapter 2. For A^+, we have

$$\frac{1}{v_g}\frac{\partial A^+}{\partial t}+\frac{\partial A^+}{\partial z}=(g^+-\alpha)A^+ \tag{3.18}$$

The equation is difficult to solve by hand because g^+ is dependent on n, which in turn is dependent on A^+. That means, (3.18) is a nonlinear partial differential equation.

However, after discretization, we only take some points on the grid, and assume the value between neighbor grids is constant and the same as the value at one neighbor grid. That means, the coefficient g^+ is no longer a variable. It is constant now, and thus equation (3.18) becomes linear in a limited space. Since the equation is linear, we can solve it by hand.

We perform changes of variables in the following way

$$z'=z \tag{3.19}$$

$$\tau=t-\frac{z}{v_g} \tag{3.20}$$

Thus

$$\begin{aligned}\frac{\partial A^+}{\partial z} &= \frac{\partial A^+}{\partial \tau}\frac{\partial \tau}{\partial z} + \frac{\partial A^+}{\partial z'}\frac{\partial z'}{\partial z} \\ &= \frac{\partial A^+}{\partial z'} - \frac{1}{v_g}\frac{\partial A^+}{\partial \tau} \qquad (3.21)\\ \frac{\partial A^+}{\partial t} &= \frac{\partial A^+}{\partial \tau}\frac{\partial \tau}{\partial t} + \frac{\partial A^+}{\partial z'}\frac{\partial z'}{\partial t} \\ &= \frac{\partial A^+}{\partial \tau} \qquad (3.22)\end{aligned}$$

Using the two equations above, (3.18) becomes

$$\begin{aligned}&\frac{1}{v_g}\frac{\partial A^+}{\partial t} + \frac{\partial A^+}{\partial z} \\ =&\frac{1}{v_g}\frac{\partial A^+}{\partial \tau} + \frac{\partial A^+}{\partial z'} - \frac{1}{v_g}\frac{\partial A^+}{\partial \tau} \\ =&\frac{\partial A^+}{\partial z'} = (g^+ - \alpha)A^+ \qquad (3.23)\end{aligned}$$

The solution of (3.23) is

$$\begin{aligned}A^+ &= u(\tau)e^{(g^+-\alpha)z'} \\ &= u\left(t - \frac{z}{v_g}\right)e^{(g^+-\alpha)z} \qquad (3.24)\end{aligned}$$

where u is any differentiable function of $\tau = t - z/v_g$.

Using (3.24), we obtain

$$\begin{aligned}A^+(z+\Delta z, t+\Delta t) &= u\left(t + \Delta t - \frac{z+\Delta z}{v_g}\right)e^{(g^+-\alpha)(z+\Delta z)} \\ &= u\left(t - \frac{z}{v_g}\right)e^{(g^+-\alpha)z}e^{(g^+-\alpha)\Delta z} \\ &= A^+(z,t)e^{(g^+-\alpha)\Delta z} \qquad (3.25)\end{aligned}$$

Here we have used the relation $\Delta t = \Delta z/v_g$.

Equation (3.25) can be applied directly to obtain the recurrence relation on discrete grids, as follows.

$$A^+_{k+1}[m+1] = A^+_k[m]\exp\left((g^+_k[m] - \alpha)\Delta z\right) \qquad (3.26)$$

Similarly, for the wave propagating backwards A^-, we have

$$\frac{1}{v_g}\frac{\partial A^-}{\partial t} - \frac{\partial A^-}{\partial z} = (g^- - \alpha)A^- \tag{3.27}$$

The solution is

$$A^- = u\left(t + \frac{z}{v_g}\right)e^{-(g^+ - \alpha)z} \tag{3.28}$$

On discrete grids, we obtain

$$A^-_{k-1}[m+1] = A^-_k[m]\exp\left((g^-_k[m] - \alpha)\Delta z\right) \tag{3.29}$$

The complete recurrence relations of this modified finite difference method include equations (3.26), (3.29), and (3.17) derived using the original finite difference method. This method can produce convergent results and is effective for this research.

It is also possible to give a natural physical interpretation for (3.26) and (3.29). Consider one point on the envelope at some time point $A^+_k[m]$. Using (3.26), we have

$$A^+_{k+1}[m+1] = A^+_k[m]\exp\left((g^+_k[m] - \alpha)\Delta z\right) = G^+_k[m]A^+_k[m] \tag{3.30}$$

$$\begin{aligned} A^+_{k+2}[m+2] &= A^+_{k+1}[m+1]\exp\left((g^+_{k+1}[m+1] - \alpha)\Delta z\right) = G^+_{k+1}[m+1]A^+_{k+1}[m+1] \\ &= G^+_{k+1}[m+1]G^+_k[m]A^+_k[m] \end{aligned} \tag{3.31}$$

$$\begin{aligned} A^+_{k+3}[m+3] &= A^+_{k+2}[m+2]\exp\left((g^+_{k+2}[m+2] - \alpha)\Delta z\right) = G^+_{k+2}[m+2]A^+_{k+2}[m+2] \\ &= G^+_{k+3}[m+3]G^+_{k+2}[m+2]G^+_{k+1}[m+1]G^+_k[m]A^+_k[m] \end{aligned} \tag{3.32}$$

$$\vdots$$

where $G^+_k[m]$ is defined as $G^+_k[m] = \exp\left((g^+_k[m] - \alpha)\Delta z\right)$. We can see from the equations above that the envelope $A^+_k[m]$ moves along the z-axis as time goes on, except for a change in the amplification. This effectively describes the propagation of wave envelope. Similar interpretation can be done on $A^-_k[m]$. This process is shown in Fig.3.3.

3.2 Simulation Program Structure

3.2.1 Recurrence Relation and Other Equations

Before we discuss the program structure, we first collect all the equations that we need in the simulation.

$$A^+_k[m+1] = \begin{cases} \sqrt{R_1}g^-_0[m]A^-_0[m] + \sqrt{1-R_1}A^i[m+1], \text{for } k = 0 \\ A^+_{k-1}[m]\exp\left((g^+_{k-1}[m] - \alpha)\Delta z\right), \text{for } k = 1, 2, \ldots, K-1 \end{cases} \tag{3.33}$$

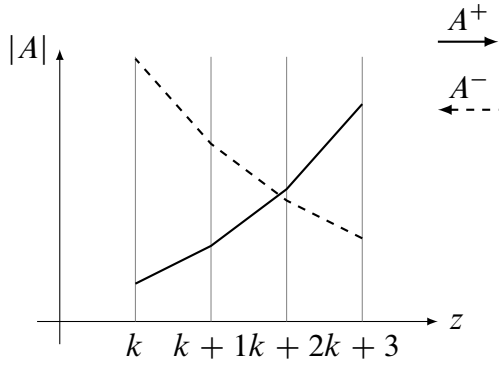

Figure 3.3: Evolution of the envelope.

$$A_k^-[m+1] = \begin{cases} A_{k+1}^-[m] \exp\left((g_{k+1}^-[m] - \alpha)\Delta z\right), \text{for } k = 0, 1, 2, \ldots, K-2 \\ \sqrt{R_2} g_{K-1}^+[m] A_{K-1}^+[m], \text{for } k = K-1 \end{cases} \tag{3.34}$$

$$n_k[m+1] = n_k[m] + \Delta t \left(\frac{J[m]}{qd} - v_g (g_k^+[m] n_{\text{ph},k}^+[m] + g_k^-[m] n_{\text{ph},k}^-[m]) - R(n_k[m]) \right) \tag{3.35}$$

$$n_{\text{ph},k}^{\pm}[m] = \frac{|A_k^{\pm}[m]|^2}{\hbar \omega w d v_g} \tag{3.36}$$

$$g_k^{\pm}[m] = \frac{\Gamma a (n_k[m] - n_0)}{1 + \varepsilon_{11} n_{\text{ph},k}^{\pm}[m] + \varepsilon_{12} n_{\text{ph},k}^{\mp}[m]} \tag{3.37}$$

$$R(n_k[m]) = A_{\text{nr}} n_k[m] + B(n_k[m])^2 + C(n_k[m])^3 \tag{3.38}$$

$$\Delta z = v_g \Delta t = \frac{L}{K} \tag{3.39}$$

The initial conditions are

$$A_k^{\pm}[0] = -100 \text{ dBm} \tag{3.40}$$

$$n_k[0] = n_0 \tag{3.41}$$

Input variables and additional output variable are

$$J[m] = \frac{I[m]}{wL} \tag{3.42}$$

$$A^i[m] = \sqrt{P_i[m]} \tag{3.43}$$

$$A^o[m+1] = \sqrt{1 - R_1} g_0^-[m] A_0^-[m] \tag{3.44}$$

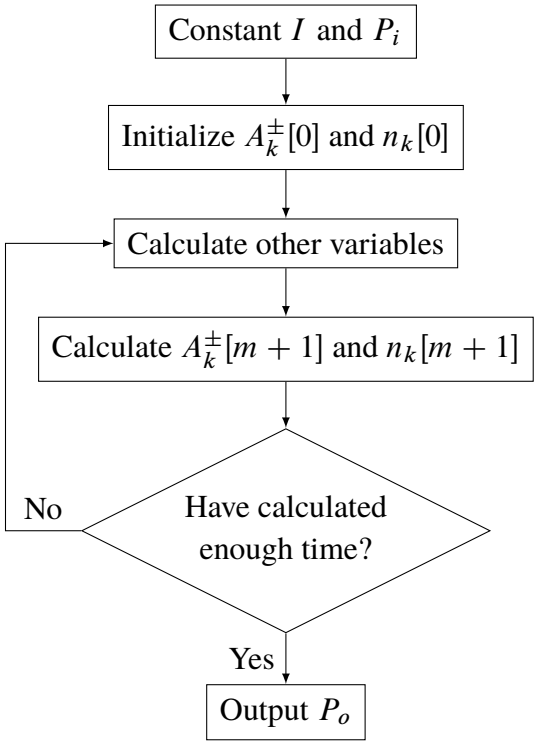

Figure 3.4: The structure of a simple subroutine to calculate the power of output light under injection of constant current and constant input light.

$$P_o[m] = |A^o[m]|^2 \tag{3.45}$$

In these equations, only (3.33), (3.34) and (3.35) are recurrence relations, and they are the most important equations in this simulation.

3.2.2 Program Structure - Subroutine

It is trivial to write a calculation subroutine in any practical programming language with the equations above. The structure of a simple implementation to calculate the power of output light after a given period under injection of constant current and constant input light is shown in Fig.3.4.

However, this kind of procedure may not be the best choice. Consider if we want to change the termination condition from running for a specific time period to obtaining a stable result. In that situation, we need to modify the program to apply the new termination condition. Or if we want to see the modulation effect, input variables will no longer be constant, and again the program needs a modification. When an optimization technique

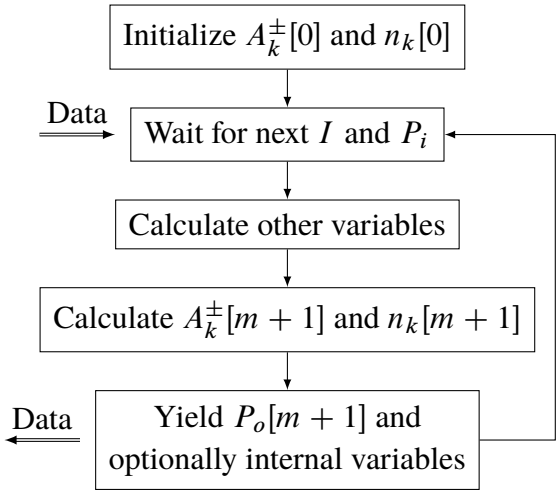

Figure 3.5: The structure of the calculation coroutine.

is implemented in the calculation, all existing subroutines need to be patched to make use of it. In a word, the subroutine method is not flexible.

3.2.3 Program Structure - Coroutine

A better solution is to use a coroutine instead of a subroutine to generate the output on request. The structure of the calculation coroutine is shown in Fig.3.5. After initialization, the coroutine waits for the values of input variables. Then the controller thread sends the values to the coroutine. The coroutine generates output variables after calculation, and waits for the next inputs.

In this way, we split the calculation process from other control commands. This separation improves the modularity of the program. The iterative way also fits well with the fact that the recurrence relation does not have any limitation in time evolution essentially. If we want, we can calculate the change in envelopes forever, even without the need of an unlimited storage. The previous subroutine can be written using the calculation coroutine, and Fig.3.6 shows the new structure.

Later we will simulate the situation when an RSOA is modulated in a loop. Other components in the loop are assumed to generate linear response, and therefore an FIFO (first in, first out) data structure is used to represent other components. The delay is represented by the length of the FIFO, and the loss is applied additionally. Besides the main controller coroutine and the calculation coroutine, another coroutine is used to generate modulation waveform from user input or random number. The program structure

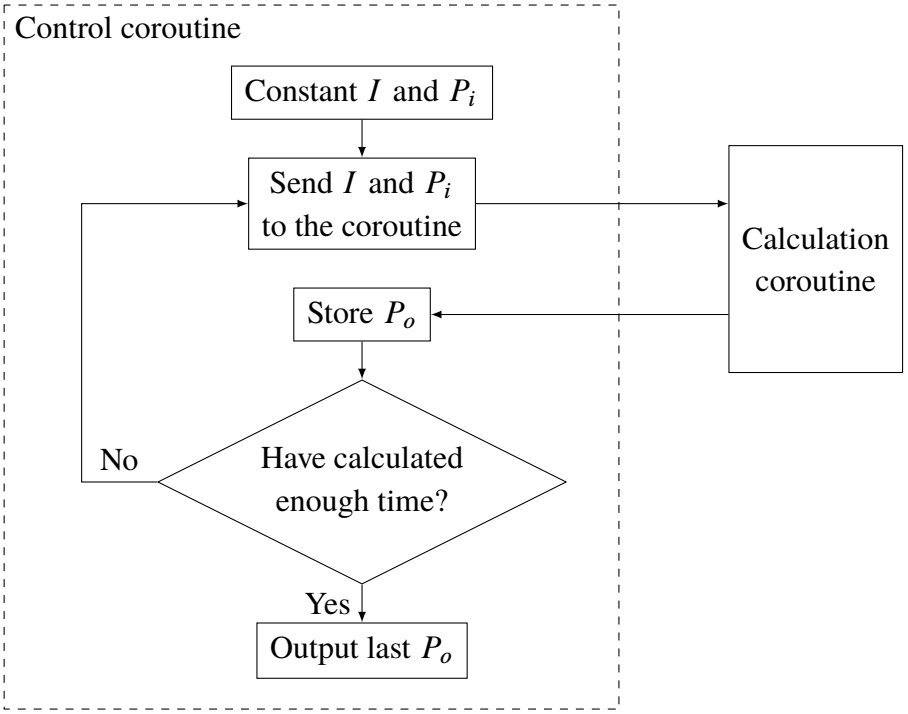

Figure 3.6: Structure to perform the task in Fig.3.4 using coroutine.

is shown in 3.7.

The coroutine way can be easily implemented in programming languages that natively support the concept of generator or coroutine, like Python and Lua, or in programming languages that have first-class continuation, like Scheme. It is also possible to implement it in simple procedural programming languages that only support function definition by saving the calculation state into a variable [18].

3.3 Parameters

The parameters used in this simulation are listed in Table 3.1. As I will show in the next chapter, these parameters fit well with a real RSOA device provided by Oclaro Japan, Inc. The choice of some parameters are based on original design parameters, while some are based on literature values and fitting effects. The grid point number is chosen so that the result does not change much when the grid point number increases.

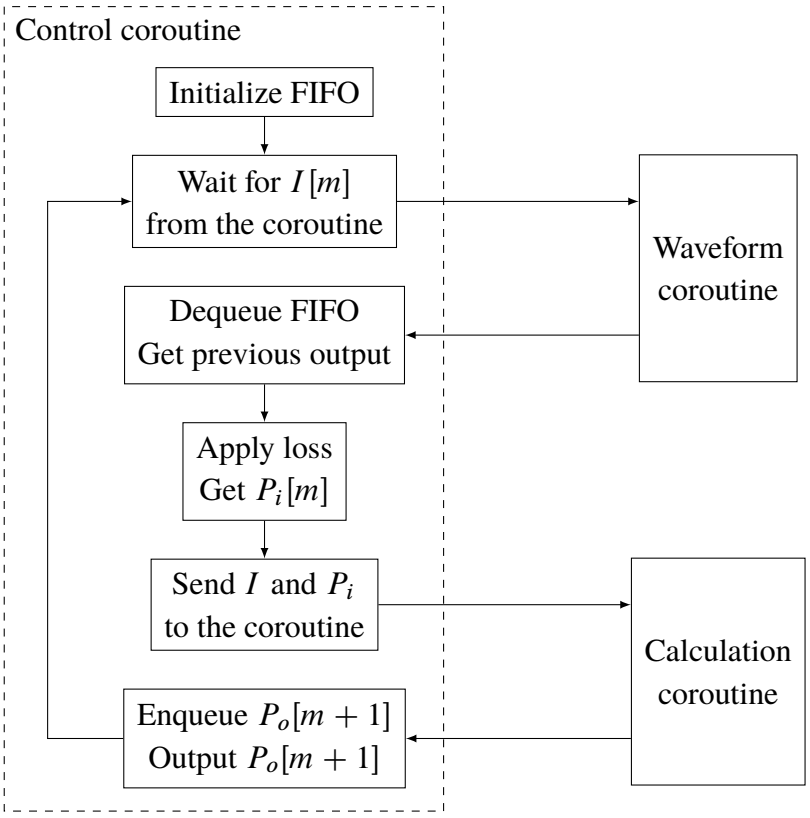

Figure 3.7: Program structure to simulate the loop using coroutine.

Table 3.1: Parameters used in the simulation.

Parameter	Symbol	Value
Wavelength	λ	$1.55\,\mu m$
Angular frequency	ω	$1.216 \times 10^{15}\,s^{-1}$
Cavity length*	L	$600\,\mu m$
Active-region width*	w	$1.7\,\mu m$
Active-layer thickness*	d	$78\,nm$
Cavity waveguide loss*	α	$20\,cm^{-1}$
Reflectivity at front facet*	R_1	0.1%
Reflectivity at rear facet*	R_2	81%
Confinement factor*	Γ	11.1%
Gain constant†	a	$1.89 \times 10^{-16}\,cm^2$
Carrier density at transparency†	n_0	$1 \times 10^{18}\,cm^{-3}$
Group refractive index†	n_g	3.4
Group velocity†	v_g	$8.82 \times 10^{7}\,m\,s^{-1}$
Nonradiative recombination rate†	A_{nr}	$5 \times 10^{8}\,s^{-1}$
Bimolecular recombination†	B	$2 \times 10^{-10}\,cm^3\,s^{-1}$
Auger recombination rate†	C	$1.2 \times 10^{-28}\,cm^6\,s^{-1}$
Self-saturation coefficient†	ε_{11}	$3.2 \times 10^{-16}\,cm^3$
Cross-saturation coefficient†	ε_{12}	$6.4 \times 10^{-16}\,cm^3$
Grid point number on z-axis	K	50
Mesh size on z-axis	Δz	$12\,\mu m$
Mesh size on t-axis	Δt	$0.136\,ps$

*Design parameters and measurement values from Oclaro Japan, Inc.
†Fitting parameters

Chapter 4

Experiments on RSOA

In this chapter we will see some experiment setups and results on RSOA. The RSOA chip I used in the experiments is provided by Oclaro Japan, Inc. This chip has a multiple-quantum well (MQW) structure (InAlGaAs wells and InAlGaAs barriers). All experiments are done at 25 °C.

4.1 Gain Saturation

In the first experiment I measured the amplification performance of the RSOA chip. The experiment setup is shown in Fig.4.1. The operating wavelength of the laser diode was 1551.4 nm. The erbium-doped fiber amplifier (EDFA) was set to operate at the automatic output signal power control (ALC) mode. In ALC mode, the output power of the EDFA is averagely constant on a time scale of millisecond order, and thus is almost constant after the laser diode (LD) is turned on. The power of light injected into the RSOA is adjusted using the attenuator.

The experimental results and corresponding simulation results are shown in Fig.4.2. The simulation results include an additional fiber coupling loss of 3.2 dB.

As shown in the figure, reasonable agreement is obtained for different values of injection current. Moreover, an additional line in the figure shows the simulation result of a single-pass SOA at injection current of 80 mA. At first, the output power of the single-pass SOA is lower than that of the RSOA. However, when input power increases, the output power increases almost linearly for a single-pass SOA, while the output power becomes gradually constant for an RSOA. We can see that the cross-gain saturation phenomenon can be effectively represented by the proposed model in this thesis.

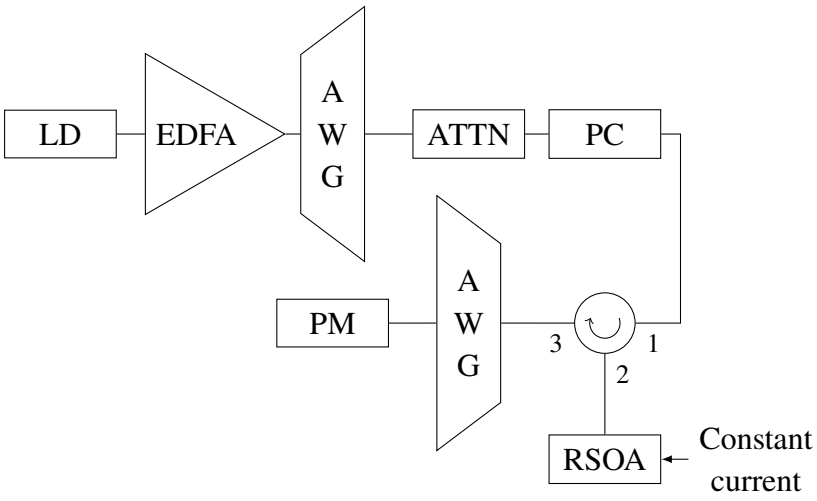

Figure 4.1: Experiment setup in Section 4.1. LD: laser diode; PC: polarization controller; EDFA: erbium-doped fiber amplifier; ATTN: optical attenuator; AWG: arrayed waveguide gratings; PM: power meter.

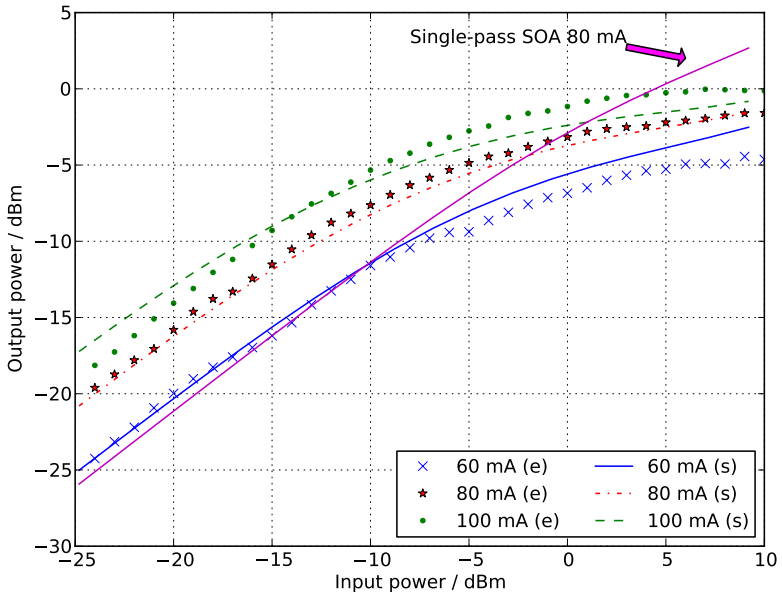

Figure 4.2: Experimental results ("e" in the figure) and simulation results ("s" in the figure) of the amplification performance of an RSOA device. The additional line shows the comparison with a single-pass SOA.

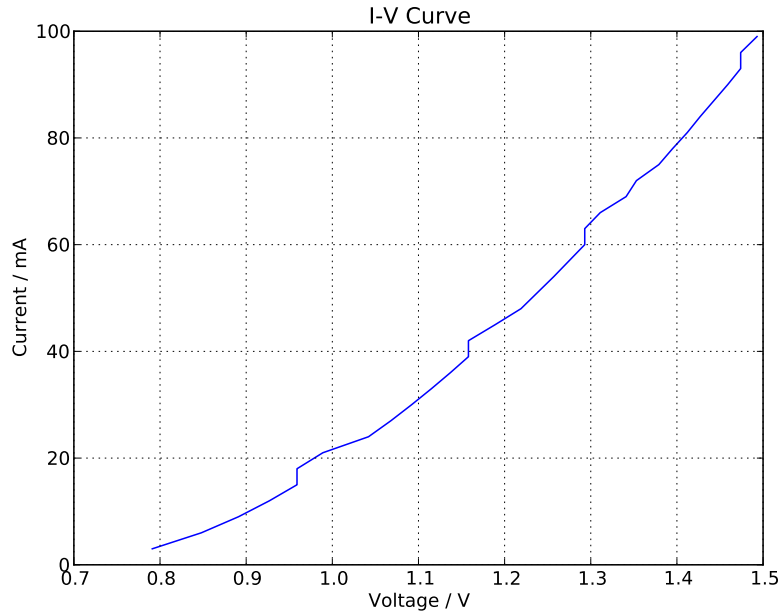

Figure 4.3: The current-voltage characteristic of the RSOA chip used in this experiment.

4.2 Current-Voltage Characteristic

The current-voltage characteristic of the RSOA chip is also measured. The results are shown in Fig.4.3.

4.3 Modulation Cancellation

We then tried to observe the modulation cancellation phenomenon. The experiment setup is shown in Fig.4.4. Constant current of 60 mA was injected into the RSOA device. The optical signal was a 2.5 Gbit/s 31 bit pseudorandom binary sequence (PRBS) non-return-to-zero (NRZ) signal with extinction ratio of 6 dB and 50% crossing percentage.

Then we changed the attenuation of the attenuator and observed the eye pattern using the oscilloscope. The results are shown in Fig.4.5.

As shown in the figure, the eye closes gradually when the input power increases. The input signal is effectively cancelled when input power enters the flat region in the output-power-versus-input-power curve. The eye-closing process has shown consistency with the amplification performance curve.

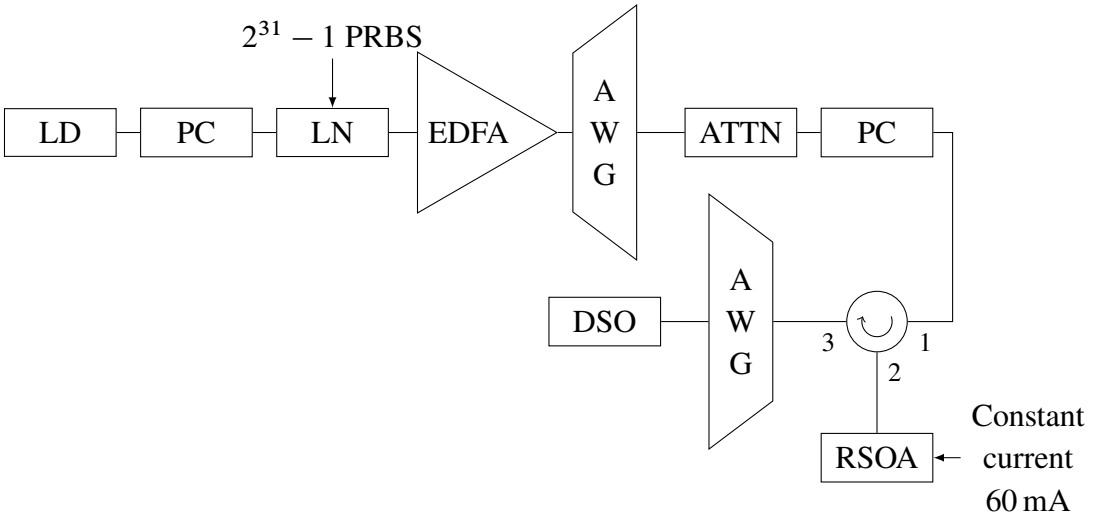

Figure 4.4: Experiment setup used in Section 4.3. LD: laser diode; PC: polarization; LN: lithium niobate electro-optic modulator; PRBS: pesudorandom binary sequence; EDFA: erbium-doped fiber amplifier; AWG: arrayed waveguide grating; ATTN: optical attenuator; DSO: digital storage oscilloscope.

4.4 WDM-PON System Operation

Finally we built a optical loop circuit to emulate the ONU transmitter part of the WDM-PON, and measured the performance of the RSOA device as a self-seeded transmitter. The experiment setup is shown in Fig.4.6. The loop is formed by using a circulator. We used an EDFA to provide additional gain because the RSOA device we used in this experiment has a relatively low gain. The optical attenuator is used to control the optical power injected into the RSOA. Isolators are used at ports of the coupler to eliminate the possible effect of reflection at optical switches.

Similar to the previous experiment, we injected a constant bias current of 80 mA into the RSOA device. At the same time, the RSOA was modulated by a 1 Gbit/s 31 bit pseudorandom binary sequence (PRBS) non-return-to-zero (NRZ) electrical signal.

Although in real application the fiber length between the ONU (RSOA) and the RN (AWG) may be several kilometers, the total fiber length in this experiment is only about 10 m. 10 m fiber will introduce a delay of over 30 bits for a 1 Gbit/s signal. Therefore we consider the delay is enough to emulate the real application.

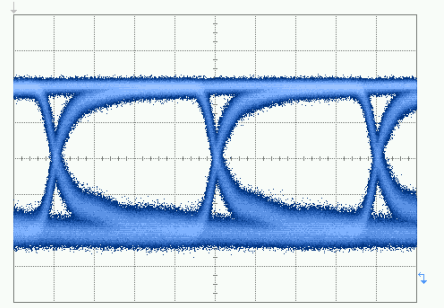

(a) Eye pattern of input optical signal.

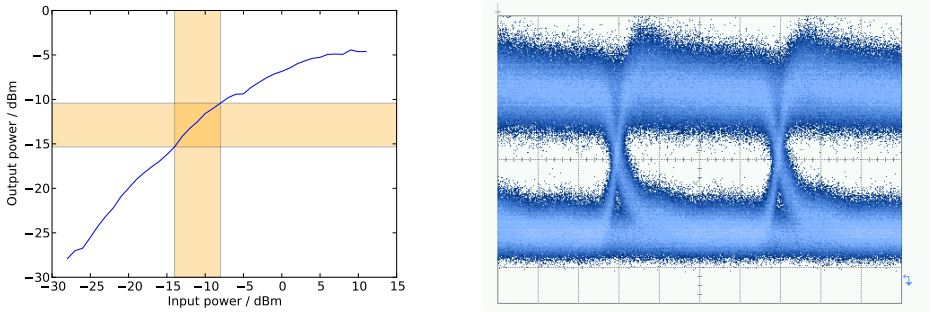

(b) When input power was -11 dBm, extinction ratio was 6 dB.

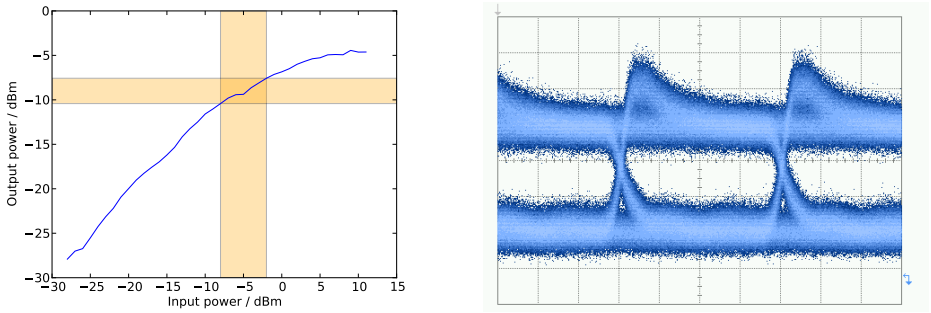

(c) When input power was -6 dBm, extinction ratio was 5.3 dB.

Figure 4.5: Experimental results in Section 4.3.

4.4.1 Establishment of Seeding Light

First we turned off the modulation on the RSOA, and measured the spectrum of RSOA's output from A in Fig.4.6. The EDFA was set to AGC mode, and the gain was 35 dB. The results are shown in Fig.4.7.

We can find ups and downs in the spectrum when the attenuator was set to a large

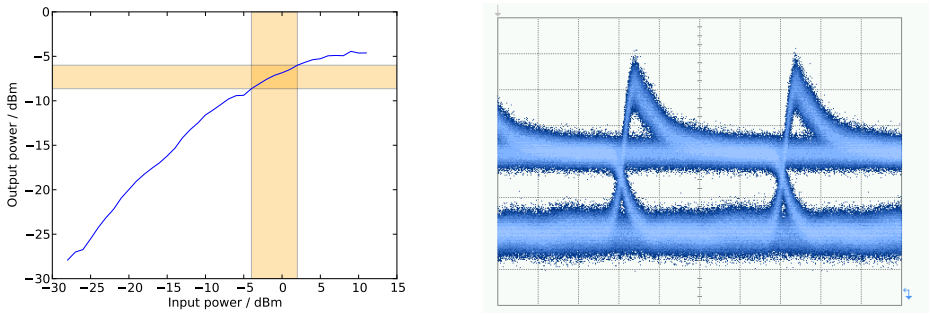

(d) When input power was -1 dBm, extinction ratio was 3.9 dB.

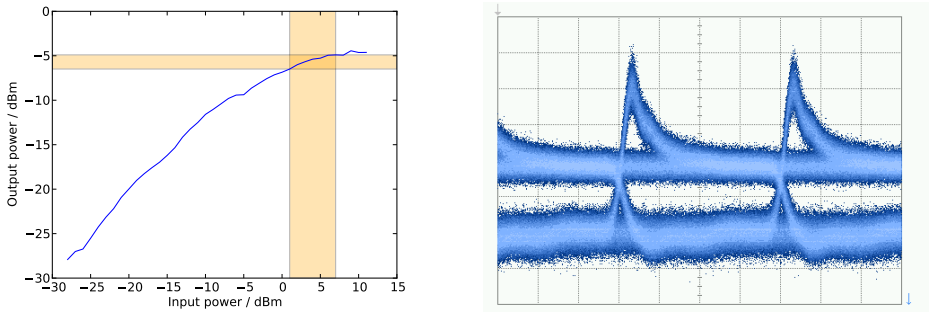

(e) When input power was 4 dBm, extinction ratio was 2.5 dB.

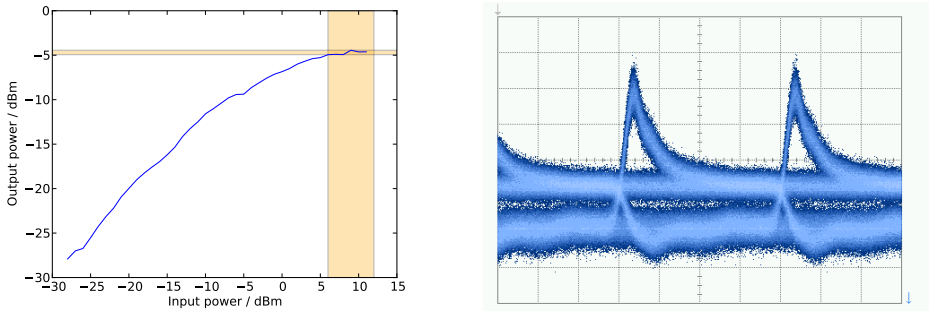

(f) When input power was 9 dBm, extinction ratio was 1.7 dB.

Figure 4.5: (continued) Experimental results in 4.3.

value (30 dB). The reason is that the RSOA device is not perfect and was at a status close to lasing. The loop attenuation was too large and the feedback was small. The loop was essentially not established. That means, the graph in fact shows the spectrum of the amplified spontaneous emission (ASE) light from the RSOA. The peak power at this state was less than −50 dBm.

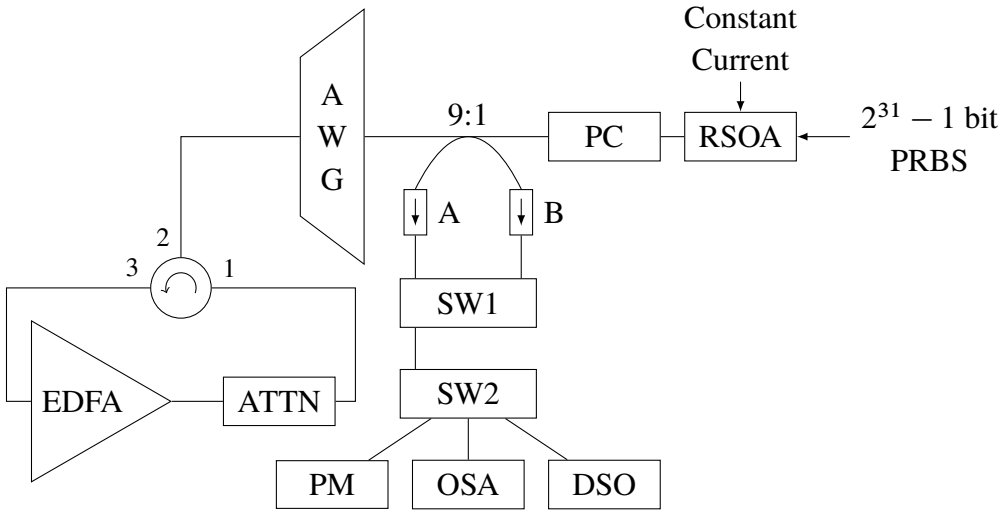

Figure 4.6: The experiment setup used in Section 4.4. The coupler is a 90%:10% coupler. PC: polarization controller; AWG: arrayed waveguide grating; EDFA: erbium-doped fiber amplifier; ATTN: optical attenuator; SW: optical switch; OSA: optical spectrum analyzer; DSO: digital storage oscilloscope; PRBS: pseudorandom binary stream.

However, when the attenuation was set to a value below 30 dB (the value depends on the port of the AWG), a peak over −30 dBm appeared in the passband of the AWG. Noticing that the large change in the spectrum was caused by only 1 dB change in the loop attenuation, we can name it *the threshold attenuation*. When the attenuation is lower than the threshold, the loop feedback is established.

When the attenuation was decreased more, the peak power kept increasing. The bandwidth of the peak also increased because of the AWG we used in this experiment has a relatively large passband.

4.4.2 Modulation

Then we turned on the modulation on the RSOA and observed the eye pattern of the RSOA's output at the coupler's A port. The EDFA was set to ALC mode, and the output power was 20 dBm. Port 4 of the AWG was used. The modulation signal has a peak-to-peak voltage of 2 V. Considering the additional resistor of 50 Ω inside high-frequency microprobe which was used inject the electrical signal into the RSOA, the modulation currents should be about 60 mA and 100 mA. The results are shown in Fig.4.8.

When the attenuation is 5 dB, we can see an open eye, although the eye is not very

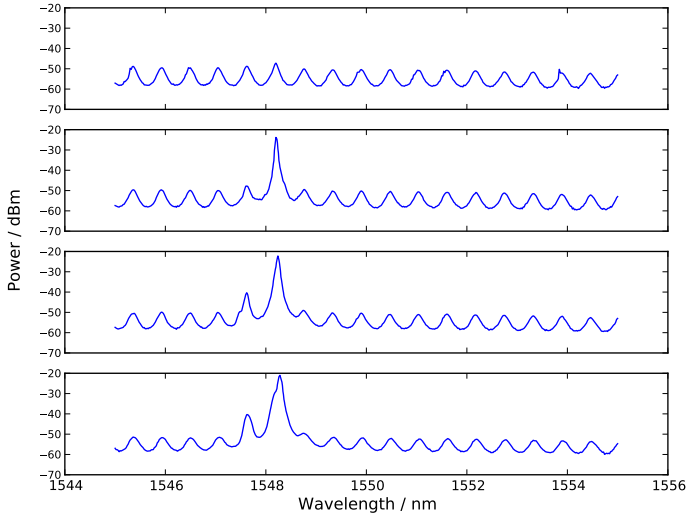

(a) AWG port 2

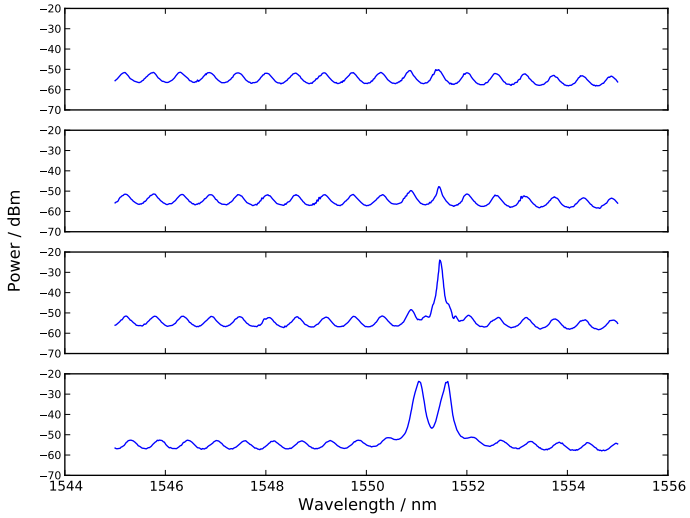

(b) AWG port 4

Figure 4.7: The spectrum graphs measured at port A of the coupler in Fig.4.6. The attenuations of the optical attenuator from top to below are (a) 30 dB, 29 dB, 25 dB and 20 dB (b) 30 dB, 28 dB, 27 dB and 20 dB respectively.

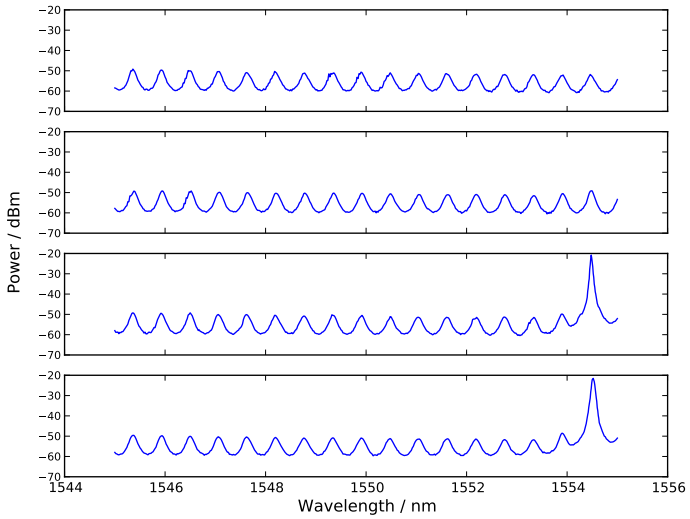

(c) AWG port 6

Figure 4.7: (continued) The spectrum graphs measured at port A of the coupler in Fig.4.6. The attenuations of the optical attenuator from top to below are (c) 30 dB, 25 dB, 24 dB and 20 dB respectively.

clear. Considerable noise sources include the instability of the coupling state between the RSOA chip and fiber, and the noise from the EDFA. When the attenuation increases, the eye gradually closes, and we cannot recognize any waveform when the input power was −10.3 dBm.

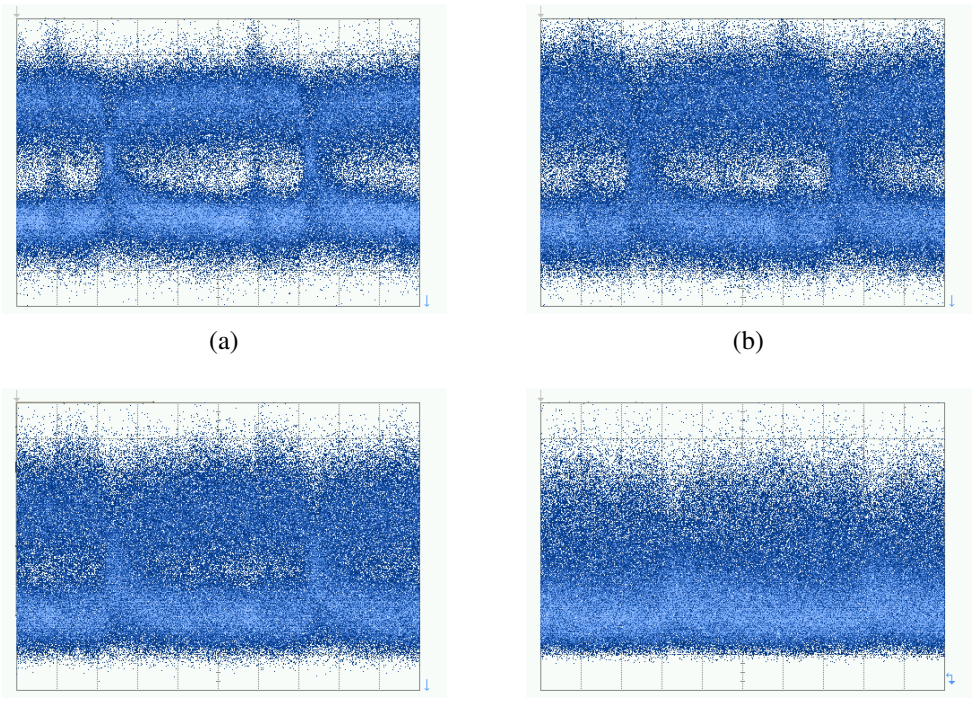

(a) (b)

(c) (d)

Figure 4.8: Eye patterns measured at port A of the coupler. The power of RSOA's injection light was (a) 4.6 dBm (b) -0.2 dBm (c) -5.1 dBm (c) -10.3 dBm.

Chapter 5

Optimization Proposals

The performance of the WDM-PON is greatly related to the amplification performance of the RSOA. When the RSOA is used as a colorless directly-modulated self-seeding transmitter, it is using the carrier light which is established during the self-seeding process. However, the carrier light is in fact carrying signals modulated previously. A key factor in the operation of the WDM-PON system is therefore how to reduce the noise from previously transmitted signals, or how to restore the *dirty* carrier light which contains previously transmitted signals to a *clean* CW carrier light.

In this chapter, I will discuss some optimization proposals of RSOA on the application as a colorless directly-modulated self-seeding transmitter. But before that, I will discuss on what property a good RSOA should have.

5.1 WDM-PON Upstream Operation Condition

5.1.1 Operating Point

First we consider how upstream signals are transmitted in a WDM-PON. If we use amplitude-shift keying (ASK) to transmit digital data, binary 0s and binary 1s should correspond to different voltages on the RSOA, or different injection currents. Here we use injection currents of 60 mA and 100 mA to represent binary 0 and 1 respectively, which is the same condition as in the experiment in Section 4.4. The amplification characteristics are plotted in Fig.5.1.

On the other hand, the output light will propagate back into the RSOA because of the existence of the reflective path. The reflective path consists of optical passive devices, and usually has good linearity. Neglecting the noise in the reflective path, we can assume

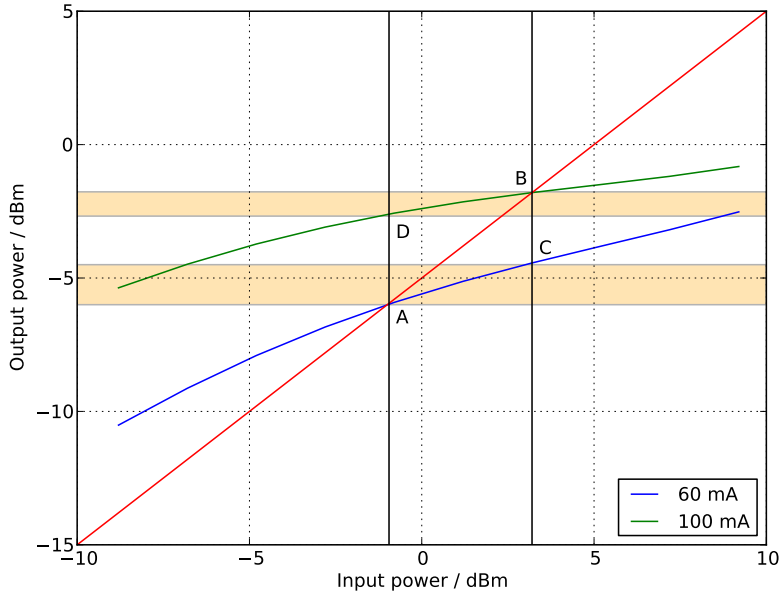

Figure 5.1: The amplification characteristics of the RSOA device and the loss curve of other components in the network.

the following linear relationship holds

$$P_o - \text{Loss} = P_i \tag{5.1}$$

where P_o and P_i are the powers of output light and input light (with respect to the RSOA) in the unit of dBm respectively. This line is also plotted in Fig.5.1. The line will have a point of intersection with RSOA's amplification characteristics curve if loss is chosen appropriately. In Fig.5.1, the points of intersection are denoted as A and B respectively.

It is easy to see that points A and B can be viewed as operating points. That means if we are not modulating the RSOA, but injecting a constant current of 60 mA or 100 mA, the system will finally become stable, and P_o and P_i will have the values as those at A or B.

5.1.2 Eye Height and Operating Point

However, we are actually modulating, and thus the system is not stable. The modulation current is not constant, and the input light is not constant, neither. Consequently, the

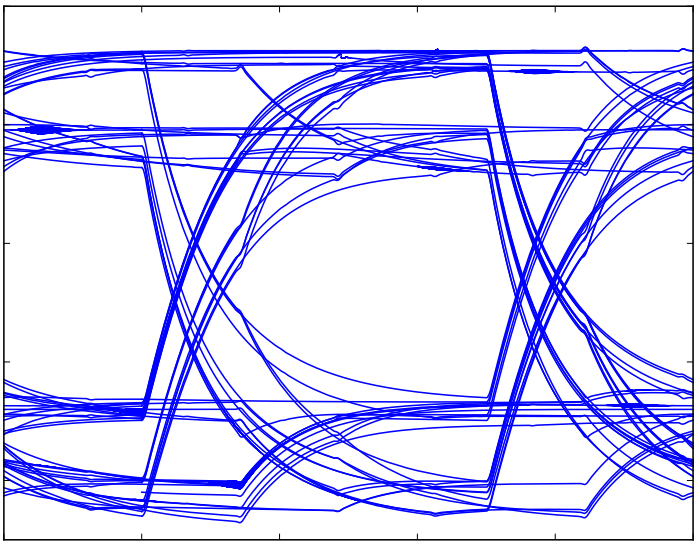

Figure 5.2: Simulated eye pattern for the modulation in Fig.5.1.

output light depends on not only the current bit we are transmitting, but also the seeding light.

For example, before the modulation begins, the system is stable at around the midpoint of AB. Soon after the modulation begins, the power of output light goes to the midpoint of BD or AC depending on the bit. Next, when light at these statuses propagate back, the power of output light will again goes elsewhere. After a long enough time, the power of input light will fill the range of $P_i(A)$ and $P_i(B)$, and the power of output light will be either between $P_o(A)$ and $P_o(C)$, or between $P_o(B)$ and $P_o(D)$.

Here we should notice that we are injecting currents of 60 mA and 100 mA when we are trying to transmit binary 0s and binary 1s respectively. Therefore for the optical carrier, binary 0s and 1s are corresponding to the bands between $P_o(A)$, $P_o(C)$ and $P_o(B)$, $P_o(D)$ respectively.

Fig.5.2 shows the simulated eye pattern for the above modulation condition. The eye height, defined as the vertical opening of the eye diagram, should be

$$\text{Eye height} = P_o(D) - P_o(C) \tag{5.2}$$

The eye height is a measure of transmission noise. A practical system must have an

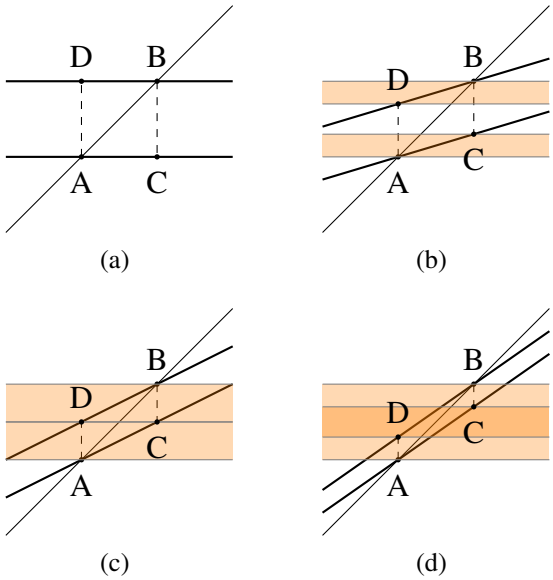

Figure 5.3: The operating points, zero level and one levels under the assumption that the amplification characteristics curves are straight lines (thick line), which have slopes of (a) 0 (b) 0.3 (c) 0.5 (d) 0.7.

open eye, and that means

$$P_o(D) > P_o(C) \tag{5.3}$$

This is a minimum requirement for the receiver to distinguish binary 0s and binary 1s. In the case in Fig.5.1, there is a difference of about 2 dB between $P_o(D)$ and $P_o(C)$.

5.1.3 Dependency of Eye Height on Curve Slope

It is important to determine where we can get an open eye, but it is difficult to obtain a precise answer because the relation between the P_o and P_i is complicated and implicit. However, noting AC and BD in Fig.5.1 are almost straight lines, we can make a good approximation by treating a local part of the amplification characteristics curve as a straight line.

Fig.5.3 shows some cases of different curve slopes under the assumption above. We can see that the best case is when slope is 0. The eye height becomes smaller when slope increases, and the eye completely closes when the slope is 0.5.

We can also see the zero level and one level from Fig.5.3. The *thicknesses* of zero level and one level increase with the increase in curve slope. An overlap region comes

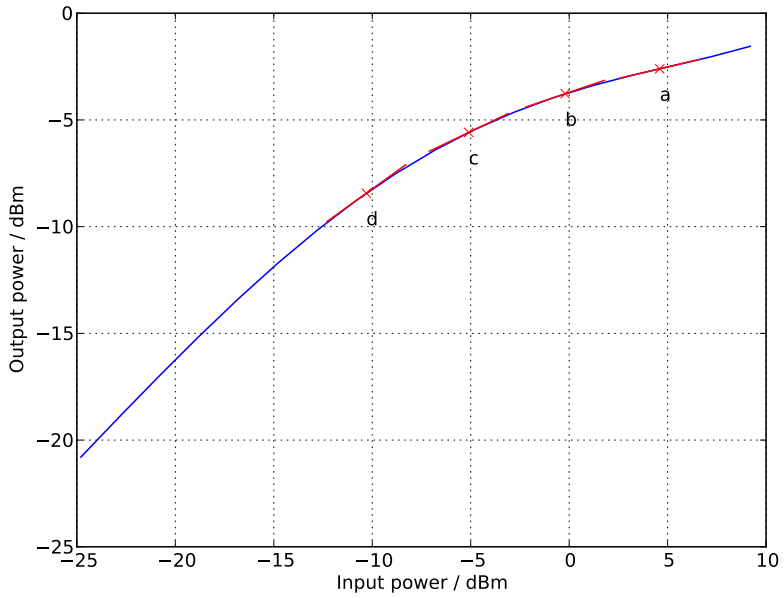

Figure 5.4: The amplification performance curve when injection current is 80 mA. The slopes are (a) 0.22 (b) 0.31 (c) 0.44 (d) 0.67 and are corresponding to the experimental results in Sec.4.4.2.

into existence when the slope is larger than 0.5. In fact, the distance between the upper bound of zero level and lower bound of one level is

$$P_o(D) - P_o(C) = (P_o(D) - P_o(A)) \cdot \frac{1-2k}{1-k} \tag{5.4}$$

where k is the slope of the curve.

Therefore, under the approximation here, the operation condition 5.3 can be rewritten as

$$\text{Slope} < 0.5 \tag{5.5}$$

It is obvious that we can get a large eye height if the slope is close to 0.

The experimental result in the previous chapter has shown agreement with this theory. Fig.4.8 has shown different eye patterns when the input power changes. We can find the operating points in Fig.5.4. For example, at point c in Fig.5.4, the slope was about 0.44. Correspondingly, in Fig.4.8, graph (c) shows a almost closed eye.

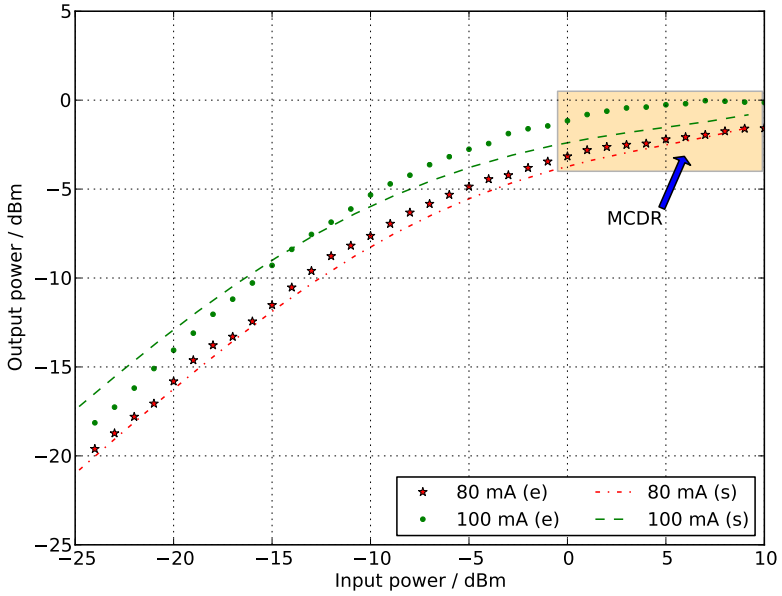

Figure 5.5: Experiment ("e" in the figure) and simulation ("s" in the figure) results of the amplification performance of the RSOA device. MCDR: modulation cancellation dynamic range.

5.1.4 Modulation Cancellation

Here we try to consider the operation from another aspect. If the signal contains a long list of consecutive binary 0s for example, the modulation current will be almost constant. However, the light input may still contain fast variations. Therefore the power of light output during this period will not be constant, and has the range that is equal to the thickness of zero level.

In the previous chapter, I measured the amplification characteristics of a typical RSOA device. The characteristics is shown in Fig.5.5. As we can see in the figure, when the power of input light falls in the orange region or is between 0 dBm and 10 dBm, the change in the power of output light will be less than about 1 dB.

This property is critical in restoring the carrier light to a *clean* status. For example, even when the carrier light is carrying a signal with extinction ratio of 6 dB, the signal will be squeezed and the extinction ratio will becomes about 1 dB after it exits the cavity of the RSOA device, as shown in the experiment in Section 4.3.

From this aspect, we can also get the conclusion that a flatter region in the amplification

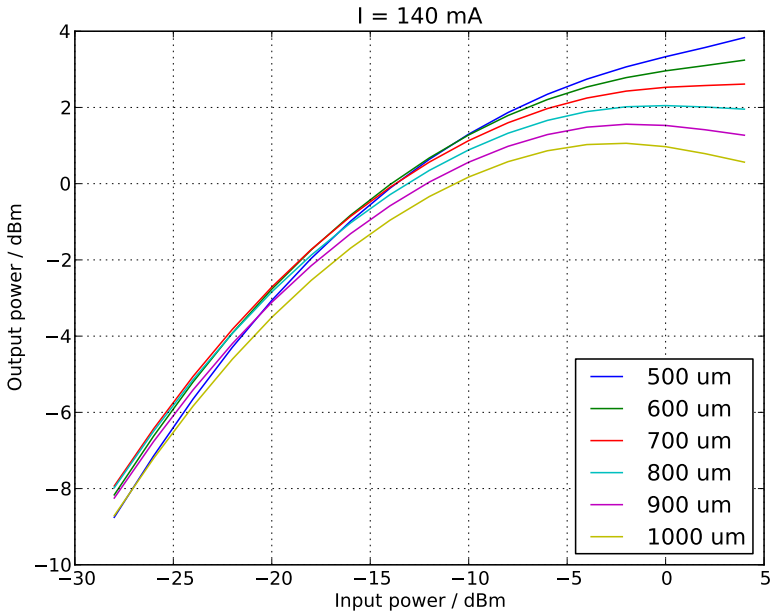

Figure 5.6: Simulated amplification performance when the cavity length changes. The injection current is fixed at 140 mA. Parameters other than cavity length L are the same as those in Table 3.1.

characteristics curve or a lower slope can lead to a better performance.

5.2 Amplification Performance

However, in previous experiments the injection light is required to have a large power, which is difficult to implement in real WDM-PONs. Since the amplification performance is the performance of the RSOA device itself, we can modify its design parameters to find the best characteristics.

5.2.1 Performance Dependency on Cavity Length

First we try to find out RSOA's amplification performance dependency on cavity length. We changed the cavity length and calculated the amplification performance using the simulator built in Chapter 3. The results are shown in Fig.5.6.

When input power is low (less than 20 dBm), the difference in the output powers of

different RSOAs is less than 1 dB, and the increase trends are also similar. The reason is that we are injecting the same current into the devices, and therefore the gains are almost the same.

However, when input power becomes large, the increase trends are different. Obviously longer devices are experiencing a stronger saturation than shorter devices at high optical inputs. For the devices with cavity lengths of 900 µm and 1000 µm, a reduction in the output power can be observed.

We can also find that the output power and the gain are smaller for longer devices at high optical injection, which may be not desirable. We should also notice that although the injection currents are the same, the current densities are different.

5.2.2 Performance Dependency on Rear-facet Reflectivity

Next we look at the effect of facet reflectivity on amplification performance. An RSOA device has two facets. The front facet, from which input light is injected and output light exits, has an anti-reflection (AR) coating, while the rear facet has a high-reflection (HR) coating. The reflectivities of the two facets are represented as R_1 and R_2 respectively.

The reflectivity of the front facet should be as low as possible. Since an RSOA device has a similar structure with a Fabry-Perot laser, it also has the possibility to start lasing. Low front-facet reflectivity increases the lasing threshold current and thus improves the device stability. In addition, low front-facet reflectivity also ensures that the light experiences a low loss when it exits the cavity.

However, there seems no special requirement on the reflectivity of the rear-facet reflectivity. Therefore we calculated different amplification performances curves when the RSOA device has different rear-facet reflectivity. The result is shown in Fig.5.7.

Clearly the output power decreases when the rear-facet reflectivity decreases. It agrees with theoretical prediction that less light will be reflected if the reflectivity becomes lower, leading to a decrease in output power finally.

What is more important is that gain saturation is stronger on devices that have lower rear-facet reflectivity. When input power is between −5 dBm and 3 dBm, the changes in output power are about 1 dB and 0.2 dB for devices with rear-facet reflectivities of 80% and 30% respectively.

5.3 Determination of Operating Points

In this chapter I have discussed about the relationship between network performance and the RSOA's amplification performance. We have seen that a lower slope around the

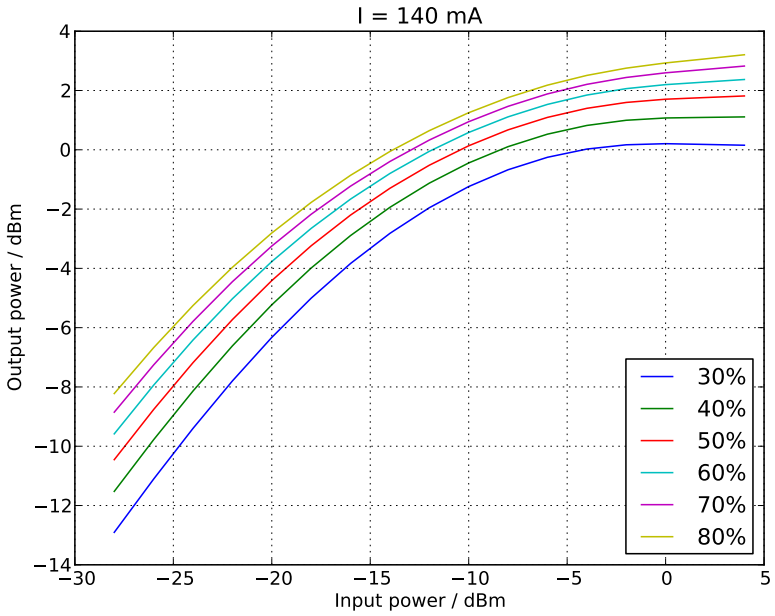

Figure 5.7: Simulated amplification performance when the rear-facet reflectivity R_2 changes. The injection current is fixed at 140 mA. Parameters other than R_2 are the same as those in Table 3.1.

operating point leads to better performance. We have also seen several parameters that may have effect on how the amplification characteristics curve looks like.

Before closing this chapter, I want to discuss again on how the operating point is determined. As written in Section 5.1.1, we just plot the amplification characteristics curve of the RSOA and a line representing the loop loss. If we keep the RSOA and modulation conditions the same but change the loop loss, we get different operating points, as shown in Fig.5.8.

As we have seen from previous simulation and experiment results, the amplification characteristics curve becomes flatter when the input power increases. If we can decrease the loop loss, the operating point are shifted to the right part, and consequently better network performance can be expected.

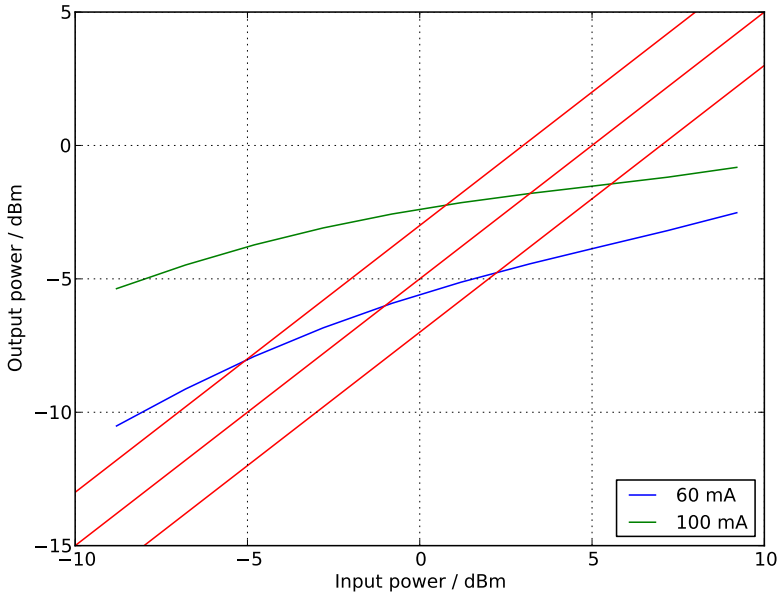

Figure 5.8: The operating points change with the loop loss.

Chapter 6

Conclusion

The purposes of this research are to discover the mechanism of the usage of reflective semiconductor optical amplifier (RSOA) as a colorless self-seeding upstream transmitter in wavelength division multiplexed (WDM) passive optical network (PON), and to propose methods to optimize the performance of the RSOA device and the network performance.

In Chapter 2, I discussed the basic theory, the rate equation theory, which is used in the analysis of RSOA. Based on recently discovered facts on RSOA, I proposed a modified gain equation which can better describe RSOA's performance. In Chapter 3, I developed a numerical method to solve the complicated rate equations. The rate equations contain a stiff partial difference equation, and therefore a special method was used to solve it effectively. A simulation program structure utilizing coroutines, which is considered more flexible than the structure utilizing subroutines, was also introduced.

In Chapter 4, I showed experimental results on the performance of an RSOA sample and the WDM-PON performance using that sample. In Chapter 5, an explanation on the mechanism of the WDM-PON based on operating points was proposed. Several optimization proposals using the simulator built in Chapter 3 were also performed.

We believe that the proposed theories in this thesis are able to explain the phenomena in practical WDM-PONs using RSOA as a colorless self-seeding upstream transmitter. The theories may also help the understanding of the mechanism of other kinds of WDM-PONs that make use of RSOA as transmitters.

Bibliography

[1] M. McGarry, M. Reisslein, and M. Maier, "Ethernet passive optical network architectures and dynamic bandwidth allocation algorithms," *Communications Surveys Tutorials, IEEE*, vol. 10, no. 3, pp. 46–60, 2008.

[2] G. Kramer and G. Pesavento, "Ethernet passive optical network (EPON): building a next-generation optical access network," *Communications Magazine, IEEE*, vol. 40, no. 2, pp. 66–73, 2002.

[3] E. Wong, "Next-generation broadband access networks and technologies," *Journal of Lightwave Technology*, vol. 30, no. 4, pp. 597–608, 2012.

[4] I. Cale, A. Salihovic, and M. Ivekovic, "Gigabit passive optical network - GPON," in *Information Technology Interfaces, 2007. ITI 2007. 29th International Conference on*, 2007, pp. 679–684.

[5] F. J. Effenberger, "The XG-PON system: cost effective 10 Gb/s access," *J. Lightwave Technol.*, vol. 29, no. 4, pp. 403–409, Feb. 2011.

[6] K. Oakley, "An economic way to see in the broadband dawn [passive optical network]," in *Global Telecommunications Conference, 1988, and Exhibition. 'Communications for the Information Age.' Conference Record, GLOBECOM '88., IEEE*, 1988, 1574–1578 vol.3.

[7] G. Agrawal and N. Dutta, *Semiconductor Lasers*. Van Nostrand Reinhold, 1993.

[8] S.-J. Park, C.-H. Lee, K.-T. Jeong, H.-J. Park, J.-G. Ahn, and K.-H. Song, "Fiber-to-the-home services based on wavelength-division-multiplexing passive optical network," *J. Lightwave Technol.*, vol. 22, no. 11, p. 2582, Nov. 2004.

[9] P. Healey, P. Townsend, C. Ford, L. Johnston, P. Townley, I. Lealman, L. Rivers, S. Perrin, and R. Moore, "Spectral slicing WDM-PON using wavelength-seeded reflective SOAs," *Electronics Letters*, vol. 37, no. 19, pp. 1181–1182, 2001.

[10] E. Wong, K. L. Lee, and T. B. Anderson, "Directly modulated self-seeding reflective semiconductor optical amplifiers as colorless transmitters in wavelength division multiplexed passive optical networks," *J. Lightwave Technol.*, vol. 25, no. 1, pp. 67–74, Jan. 2007.

[11] L. Marazzi, P. Parolari, M. Brunero, A. Gatto, M. Martinelli, R. Brenot, S. Barbet, P. Galli, and G. Gavioli, "Up to 10.7-Gb/s high-PDG RSOA-based colorless transmitter for WDM networks," *Photonics Technology Letters, IEEE*, vol. 25, no. 7, pp. 637–640, 2013.

[12] P. Chanclou, F. Payoux, T. Soret, N. Genay, R. Brenot, F. Blache, M. Goix, J. Landreau, O. Legouezigou, and F. Mallécot, "Demonstration of RSOA-based remote modulation at 2.5 and 5 Gbit/s for WDM PON," in *Optical Fiber Communication Conference and Exposition and The National Fiber Optic Engineers Conference*, Optical Society of America, 2007, OWD1.

[13] S. O'Duill, L. Marazzi, P. Palolari, W. Freude, C. Koos, and J. Leuthold, "Modulation cancellation properties of reflective SOAs," in *European Conference and Exhibition on Optical Communication*, Optical Society of America, 2012, We.2.E.1.

[14] J.-M. Kang, T.-Y. Kim, I.-H. Choi, S.-H. Lee, and S.-K. Han, "Self-seeded reflective semiconductor optical amplifier based optical transmitter for up-stream WDM-PON link," *Optoelectronics, IET*, vol. 1, no. 2, pp. 77–81, Apr. 2007.

[15] G. Agrawal and N. Olsson, "Self-phase modulation and spectral broadening of optical pulses in semiconductor laser amplifiers," *Quantum Electronics, IEEE Journal of*, vol. 25, no. 11, pp. 2297–2306, Nov. 1989.

[16] M. Takenaka, "Study on all-optical flip-flop using bistable laser diodes with nonlinear couplers," PhD thesis, Department of Electronic Engineering, The University of Tokyo, 2002.

[17] C. Grossmann and H.-G. Roos, *Numerical treatment of partial differential equations*. Springer, 2007.

[18] H. ABELSON, G. SUSSMAN, and J. SUSSMAN, *Structure and Interpretation of Computer Programs, 2nd Edition*, ser. The Mit electrical engineering and computer science series. Mit Press, 1996.

List of Publication

[1] Y. Zeng, S. Yamauchi, T. Tanemura, and Y. Nakano, “Numerical and experimental study on reflective semiconductor optical amplifier for self-seeded WDM-PON application,” in *IEICE Society Conference*, 2013, accepted.

Acknowledgement

This work could not be accomplished without the support from many people.

I owe my deepest gratitude to my supervisor Professor Yoshiaki Nakano. Without his support, I could not come to Japan, and this work would hardly have been completed. I also express my warmest gratitude to Associate Professor Takuo Tanemura, who suggested this topic to me. His supervision in experiment operations and guidance in the interpretation of simulation and experimental results have been essential during this work.

I am deeply grateful to Kazuhisa Uomi, PhD, Hiroaki Inoue, PhD, Atsushi Takai, PhD, Kenji Uchida, Dr. Eng. and Mr. Syunya Yamauchi from Oclaro Japan, Inc. for the providence of RSOA samples and kind advice on this study. I want to express my special gratitude to Mr. Syunya Yamauchi for his assistance on experiment operations.

I want to express my gratitude to Associate Professor Masakazu Sugiyama, Akio Higo, PhD, Wang Yunpeng, PhD and Kentarou Watanabe, PhD for their discussions on group meetings. I also owe a great debt of gratitude to Mr. Masaru Zaitsu, Mr. Hiromasa Fujii and all other lab members, including those who left the lab before my graduation, for their enormous help, moral support, motivation and kindness.

Finally and most importantly, I would like to thank my parents for their support and encouragement throughout this study.

Zeng Yuxiao
August 10, 2013